nature cell biology

Proteomic mapping of ER–PM junctions identifies STIMATE as a regulator of Ca^{2+} influx

Ji Jing[1,8], Lian He[1,8], Aomin Sun[2,8], Ariel Quintana[3,8], Yuehe Ding[4,8], Guolin Ma[1], Peng Tan[1], Xiaowen Liang[1], Xiaolu Zheng[5], Liangyi Chen[5], Xiaodong Shi[6], Shenyuan L. Zhang[7], Ling Zhong[1], Yun Huang[1], Meng-Qiu Dong[4], Cheryl L. Walker[1], Patrick G. Hogan[3], Youjun Wang[2,9] and Yubin Zhou[1,7,9]

Specialized junctional sites that connect the plasma membrane (PM) and endoplasmic reticulum (ER) play critical roles in controlling lipid metabolism and Ca^{2+} signalling[1–4]. Store-operated Ca^{2+} entry mediated by dynamic STIM1–ORAI1 coupling represents a classical molecular event occurring at ER–PM junctions, but the protein composition and how previously unrecognized protein regulators facilitate this process remain ill-defined. Using a combination of spatially restricted biotin labelling *in situ* coupled with mass spectrometry[5,6] and a secondary screen based on bimolecular fluorescence complementation[7], we mapped the proteome of intact ER–PM junctions in living cells without disrupting their architectural integrity. Our approaches led to the discovery of an ER-resident multi-transmembrane protein that we call STIMATE (*STIM*-activating enhancer, encoded by *TMEM110*) as a positive regulator of Ca^{2+} influx in vertebrates. STIMATE physically interacts with STIM1 to promote STIM1 conformational switch. Genetic depletion of STIMATE substantially reduces STIM1 puncta formation at ER–PM junctions and suppresses the Ca^{2+}–NFAT signalling. Our findings enable further genetic studies to elucidate the function of STIMATE in normal physiology and disease, and set the stage to uncover more uncharted functions of hitherto underexplored ER–PM junctions.

ER–PM junctions are defined as spatially extended or small circular compartments in which the PM and ER membranes are stably separated at a distance of approximately 10–20 nm without direct membrane fusion[1]. The broad significance of this structure has only recently begun to be appreciated, with emerging roles in lipid metabolism and Ca^{2+} homeostasis[1–4]. Although ER–PM junctions were first observed over half a century ago[8], systematic dissection of this specialized subcompartment at the molecular level remains challenging owing to the lack of appropriate methods and convenient tools, which motivated us to explore a non-biased yet effective approach to obtain an integrated picture of ER–PM junctions. By taking advantage of an *in situ* protein labelling technique[5,6], we set out to map the proteome of ER–PM junctions that are dedicated to store-operated calcium entry (SOCE), a fundamental physiological process that is mediated by two protein families, STIM and ORAI (ref. 3). The ER-resident Ca^{2+} sensor protein STIM1, when fused to an engineered ascorbate peroxidase 2 (APEX2), enables proximity biotin labelling with least perturbation to the architecture of ER–PM junctions, thereby opening new avenues for capturing protein complexes situated at or in close proximity of STIM1 in living cells (Fig. 1a). At the heart of this *in situ* protein labelling technique is APEX2-catalysed conversion of biotin–phenol in the presence of H_2O_2 to phenoxyl radicals, which could attack electron-rich amino acids and covalently attach biotin tags to targeted proteins[5,6]. Biotinylated proteins can be subsequently enriched by streptavidin beads and analysed by mass spectrometry. Notably, these radicals have very short lifetimes (<1 ms) with an estimated labelling radius of <20 nm (refs 5,9,10), thus matching the distance that separates ER and PM at junctional sites. One additional benefit of this approach is that it enables dynamic sampling of this specialized cellular compartment during the translocation of STIM1 from ER towards PM, thereby allowing us to compare protein complexes surrounding STIM1 before and after store depletion.

Following ER Ca^{2+} depletion elicited by thapsigargin, a blocker of the sarco/endoplasmic reticulum Ca^{2+} ATPase (SERCA), total internal reflection fluorescence (TIRF) microscope imaging showed

[1]Institute of Biosciences and Technology, Texas A&M University Health Science Center, Houston, Texas 77030, USA. [2]Beijing Key Laboratory of Gene Resource and Molecular Development, College of Life Sciences, Beijing Normal University, Beijing 100875, China. [3]Division of Signaling and Gene Expression, La Jolla Institute for Allergy and Immunology, La Jolla, California 92037, USA. [4]National Institute of Biological Sciences, Beijing 102206, China. [5]Institute of Molecular Medicine, Peking University, Beijing 100871, China. [6]Department of Chemistry, West Virginia University, Morgantown, West Virginia 26506, USA. [7]Department of Medical Physiology, College of Medicine, Texas A&M University Health Science Center, Temple, Texas 76504, USA. [8]These authors contributed equally to this work.
[9]Correspondence should be addressed to Y.W. or Y.Z. (e-mail: wyoujun@bnu.edu.cn or yzhou@ibt.tamhsc.edu)

Received 18 February 2015; accepted 29 July 2015; published online 31 August 2015; DOI: 10.1038/ncb3234

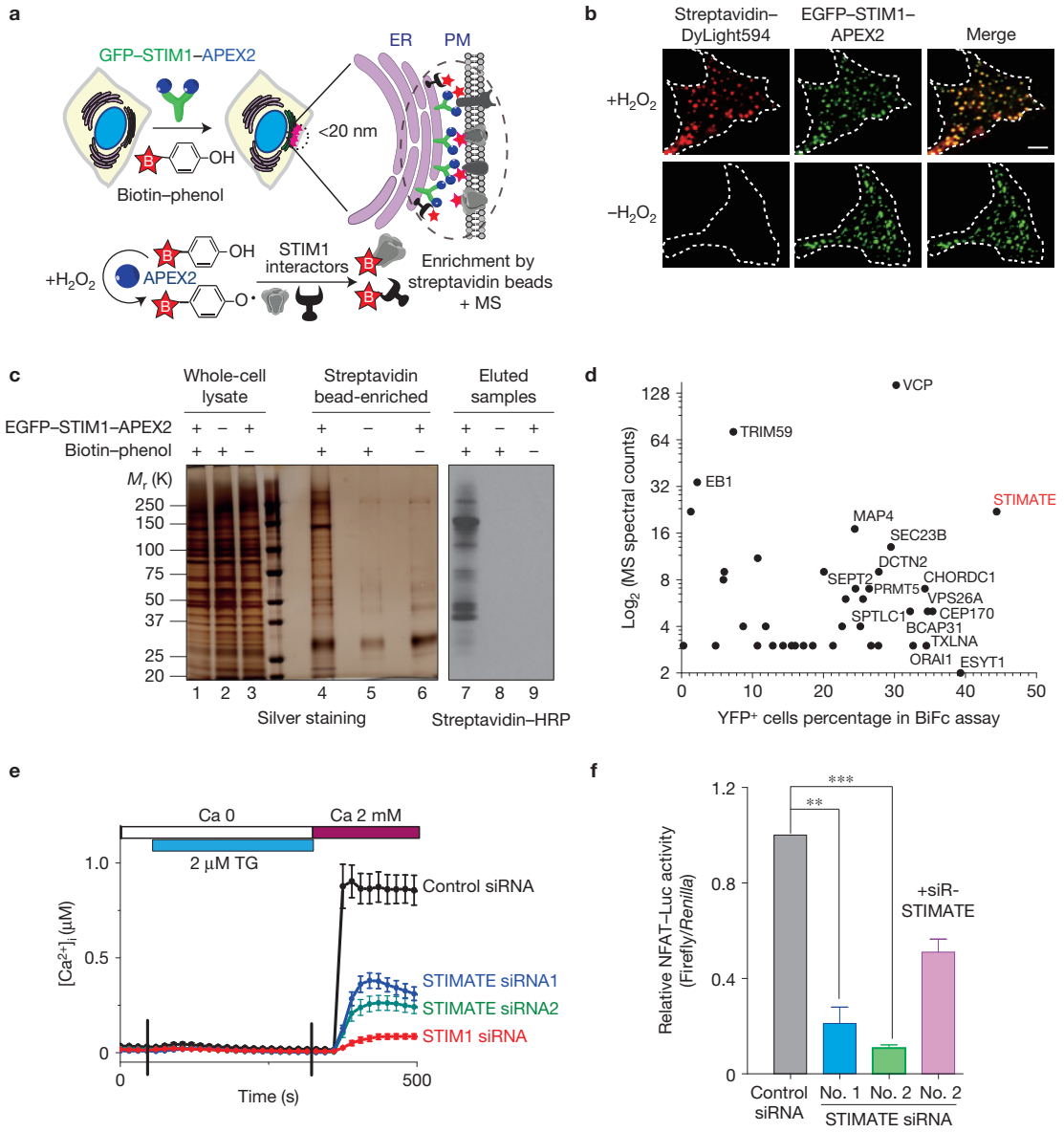

Figure 1 STIMATE identified as a positive regulator of the Ca^{2+}–NFAT pathway. (**a**) Schematic depiction of proteomic mapping of potential STIM1 interactors at ER–PM junctions through APEX2-mediated biotin labelling *in situ*. APEX2 fused to STIM1 enables biotin labelling on proteins located <20 nm from STIM1. This reaction requires externally added H_2O_2. Biotinylated proteins were further affinity-enriched with streptavidin beads, with the eluted products analysed by mass spectrometry (MS). (**b**) Fluorescence imaging of biotinylated proteins (stained with streptavidin conjugated with Dylight594) in HEK293 cells expressing GFP–STIM1–APEX2 as illustrated in **a**. Store depletion was induced by 1 μM thapsigargin (TG) in nominally Ca^{2+}- and serum-free medium. Scale bar, 5 μm. (**c**) Silver staining and immunoblotting of biotinylated protein complexes surrounding STIM1 puncta at ER–PM junctions. Shown on the SDS–PAGE are samples before (lanes 1–3) and after (lanes 4–6) streptavidin bead enrichment, as well as the eluted samples immunoblotted by streptavidin conjugated by horseradish peroxidase (streptavidin–HRP, lanes 7–9). (**d**) Scatter plot of identified potential STIM1-binding partners. BiFc (Supplementary Fig. 1a–c) was used as a secondary assay to confirm strong hits that emerged from the proteomic study. The amino-terminal fragment of YFP (YFP_N, residues 1–155) is fused to the STIM1 C terminus as the bait to interact with prey in a customized library containing candidate genes fused with the C-terminal half of YFP (YFP_C, residues 156–238). Each candidate was plotted according to its MS spectral counts (*Y* axis) and the degree of YFP fluorescence restoration (*X* axis, as shown in Supplementary Fig. 1c). (**e**) Thapsigargin-induced Ca^{2+} influx in HEK293 cells transfected with control siRNA ($n=30$), STIMATE siRNA oligonucleotide 1 ($n=34$), STIMATE siRNA oligonucleotide 2 ($n=45$) or STIM1 siRNA ($n=60$ cells pooled across three independent experiments). Error bars denote s.e.m. (**f**) Quantification of NFAT-dependent luciferase activity in HEK293 cells treated with the indicated siRNA oligonucleotides or co-transfected with an siRNA-resistant STIMATE construct (siR-STIMATE). $^{**}P<0.01$; $^{***}P<0.001$ (paired Student's *t*-test). Error bars denote s.d. for $n=12$ wells of cultured cells (0.1–0.5 million cells per well) pooled across three independent experiments. Unprocessed original scans of blots/gels are shown in Supplementary Fig. 6.

that EGFP-tagged STIM1–APEX2 formed puncta and co-localized tightly with biotinylated proteins, the latter of which were labelled by fluorophore-conjugated streptavidin (Fig. 1b). This process was dependent on H_2O_2 because biotinylation was not observed when omitting H_2O_2 in the reaction medium. The H_2O_2- and APEX2-dependent biotinylation of protein complexes surrounding STIM1

was further confirmed by silver staining after affinity enrichment and independently by western blotting probed by streptavidin–HRP (Fig. 1c). As ORAI1 (relative molecular mass, 33,000 (M_r 33K)) is a known binding partner of STIM1, we first analysed a gel slice corresponding to M_r 25K–37K on the SDS–PAGE with mass spectrometry in our initial experiment and confirmed the presence of ORAI1 using liquid chromatography coupled to tandem mass spectrometry (LC–MS/MS). In the same gel band, we repeatedly detected the gene product of *TMEM110* (RefSeq ID: NM_198563), hereafter designated as STIMATE (for *STIM*-activating enhancer, Supplementary Fig. 1). In our subsequent LC–MS/MS analyses on all of the eluted products, we further identified a total of 73 potential STIM1 interactors, with 17 detected in both store-full and store-depleted HEK293 cells (Supplementary Tables 1 and 2). Most of them fell into the categories of ER- or PM-resident proteins, cytoskeletal components, and proteins functioning in intracellular membrane trafficking or post-translational modifications. Notably, 18% of them also appeared as strong hits identified in an independent genome-wide screen for regulators of nuclear factor of activated T-cells (NFAT; ref. 11), a transcriptional factor that is downstream of Ca^{2+} influx mediated by STIM–ORAI signalling. The prowess of this approach was further attested by the identification of EB1, SERCA2, ORAI1, voltage-dependent Ca^{2+} channels, extended synaptotagmin 1 and septins as candidate proteins that are in close proximity to STIM1 (Supplementary Tables 1 and 2). These proteins are known to either directly interact with STIM1 or reside in the ER–PM junctions[3,11–21].

Given the major interest in identifying protein regulators at ER–PM junctions that are directly involved in STIM1-dependent Ca^{2+} influx, we created a customized prey library of 38 genes representing most gene products (for example, STIMATE) identified under both store-full (resting) and store-depleted conditions, as well as candidate genes that have an annotated function in Ca^{2+} signalling or harbour predicted transmembrane domains (Supplementary Table 3). A secondary screen based on bimolecular fluorescence complementation (BiFc, Supplementary Fig. 1a–c) was performed to examine their potentials as STIM1 interactors either before or after thapsigargin-induced store depletion. Our assay is based on the reconstitution of an intact yellow fluorescent protein (YFP) from two complementary non-fluorescent fragments when they are brought together through STIM1 and STIM1-binding partners. Again, STIMATE stood out as one of the strongest hits in the screen (Fig. 1d and Supplementary Fig. 1b,c). Taken together, STIMATE, a positive regulator of NFAT activation identified in a previous genome-wide RNAi screening[11], emerged early and prominently in both screens, which prompted us to further examine its role in modulating Ca^{2+} flux at ER–PM junctions, and in parallel, to dissect the molecular mechanism underlying its interplay with STIM1.

To examine the effect of STIMATE on SOCE and its downstream effectors, we monitored the Ca^{2+} flux and NFAT-dependent activities by treating HEK293 cells with siRNA oligonucleotides designed to specifically target STIMATE. The knockdown efficiency (~60–80%) of two synthesized STIMATE siRNA oligonucleotides was confirmed by quantitative PCR (Supplementary Fig. 2). As shown in Fig. 1e,f, thapsigargin-triggered SOCE, as well as NFAT-dependent luciferase activity, was significantly suppressed in HEK293 cells transfected with either of the two STIMATE siRNA oligonucleotides. The inhibitory effect could be rescued in STIMATE-siRNA-treated cells by overexpression of an siRNA-resistant variant of STIMATE (Fig. 1f).

To further demonstrate the role of STIMATE in modulating SOCE, we generated STIMATE knockout (STIMATE-KO) HEK293 stable cell lines by disrupting exon 4 of human *STIMATE* with the CRISPR/Cas9 genome-editing tool[22]. Gene disruption was validated using both the Surveyor nuclease assay and Sanger's sequencing of exon 4 (Supplementary Fig. 2c,d). In two stable STIMATE-KO clones harbouring early stop codons, the cytoplasmic Ca^{2+} increase in response to ionomycin-induced store depletion (Supplementary Fig. 2e) was profoundly reduced, whereas the Ca^{2+} release from the ER Ca^{2+} store remained largely unaltered (first peak, Supplementary Fig. 2e). Together, these results suggest that STIMATE is a previously unrecognized positive modulator of SOCE.

STIMATE is broadly expressed in mouse and human tissues (Supplementary Fig. 2a). The STIMATE protein is predicted to contain multiple putative transmembrane segments with a polybasic C-tail (Fig. 2a and Supplementary Fig. 1d), but its subcellular localization and membrane topology remain unknown. When overexpressed in HEK293, HeLa or COS-7 cells, STIMATE localized to ER and overlapped tightly with the ER marker Sec61β (ref. 23) or DsRed–ER (Fig. 2b and Supplementary Fig. 3). Interestingly, STIMATE exhibited a predominant PM-like localization with a small pool trapped intracellularly when the last 74 amino acids were truncated ($STIMATE_{1–220}$, Fig. 2a). Through a serial truncation study combined with site-directed mutagenesis, we further mapped a region (residues ^{241}KXRXRR^{246}) that seems to be critical for keeping STIMATE localized within the ER. Substitution of these positively charged residues with glutamines (K or R>Q mutant) caused a large fraction of the ER-resident $STIMATE_{1–250}$–mCherry to exhibit a PM-like distribution (Fig. 2a). Next, we performed a chemical crosslinking experiment to examine the oligomeric state of STIMATE. As shown in Fig. 2c, addition of the membrane-permeable crosslinker DSS resulted in the appearance of protein bands corresponding to multimers of STIMATE on SDS–PAGE, suggesting that STIMATE could be assembled as oligomers in ER membrane. This result echoes the presence of a GXXXG transmembrane association motif[24] in one of its predicted transmembrane segments (Supplementary Fig. 1d). The tendency of STIMATE to multimerize was further attested by the efficient restoration of YFP fluorescence when STIMATE was carboxy-terminally tagged with two complementary non-fluorescent YFP fragments in the BiFc assay (Supplementary Fig. 1b,c). The membrane topology of STIMATE was further determined by using a fluorescence protease protection assay[25] with EGFP–STIM1 and STIM1–YFP as controls. We found that both termini of STIMATE face towards the cytosolic side of ER (Supplementary Fig. 1e–h).

We next examined whether STIMATE is located in the vicinity of the two main players of SOCE, STIM1 and ORAI1. When expressed together with ORAI1 or STIM1 in HEK293 cells, STIMATE co-localized tightly with STIM1 to ER but not with ORAI1 at resting conditions (Fig. 2d), a finding that is further corroborated by results from an independent fluorescence resonance energy transfer (FRET) assay (Fig. 2e). Discernible FRET signals were detected only in HEK293 cells co-transfected with CFP–STIMATE and STIM1–YFP but not in cells coexpressing CFP–STIMATE and ORAI1–YFP (Fig. 2e). When expressed alone or coexpressed with an ER

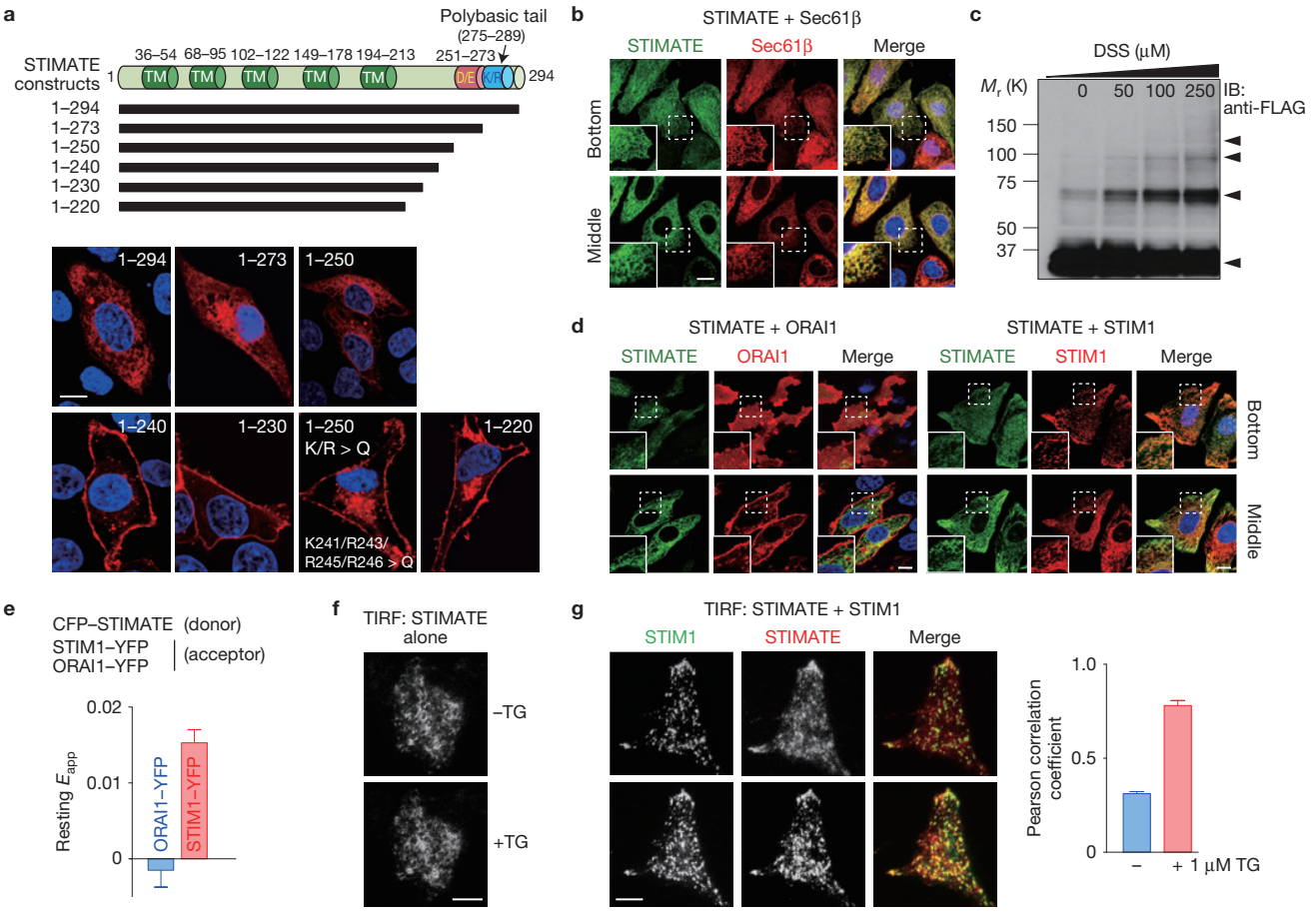

Figure 2 STIMATE is an ER-resident protein that co-localizes with STIM1. (**a**) Predicted domain architecture of STIMATE and confocal images of indicated STIMATE variants tagged with a C-terminal mCherry. STIMATE is predicted to contain 4–5 transmembrane segments (see Supplementary Fig. 1). TM, predicted transmembrane segment. D/E: a negatively charged region in the C terminus of STIMATE (STIMATE-CT). K/R: a polybasic domain in STIMATE-CT. Blue, nuclear staining with Hoechst 33342. Scale bar, 10 μm. (**b**) Confocal sections (at the footprint or the middle plane) of HEK293 cells coexpressing EGFP–STIMATE (green) and the ER marker mCherry–Sec61β (red). Nuclei were labelled in blue by Hoechst 33342. The insets show the regions outlined by dashed lines at higher magnification. Scale bar, 10 μm. (**c**) Crosslinked FLAG–STIMATE resolved on SDS–PAGE. FLAG-tagged STIMATE was transiently expressed in HEK293 cells and subjected to chemical crosslinking with 0–250 μm DSS (a membrane-permeable crosslinker) on ice for 5 min. The arrowheads indicate the appearance of FLAG–STIMATE oligomers on crosslinking. (**d**) Confocal images of EGFP–STIMATE in HEK293 cells coexpressing mCherry–ORAI1 or mCherry–STIM1 without store depletion. Blue, nuclear staining with Hoechst 33342. Scale bar, 10 μm. (**e**) Quantification of FRET signals in HEK293 cells coexpressing CFP–STIMATE with ORAI1–YFP ($n = 5$ cells) or with STIM1–YFP ($n = 10$ cells) pooled across three independent experiments. Error bars denote s.e.m. (**f**) Representative TIRF images of an HEK293 cell expressing STIMATE–EYFP before and after store depletion induced by 1 μM thapsigargin (TG). Scale bar, 10 μm. (**g**) Representative TIRF images of an HEK293 cell coexpressing EGFP–STIM1 (green) and mCherry–STIMATE (red) before and after store depletion induced by 1 μM thapsigargin. The single-channel images are shown in greyscale. The plot on the right shows the quantification of STIM1–STIMATE co-localization under TIRF microscopy by Pearson's correlation coefficient. Error bars denote s.e.m. for $n = 6$ cells pooled across two independent experiments. Scale bar, 10 μm. Unprocessed original scans of blots/gels are shown in Supplementary Fig. 6.

marker in HEK293, HeLa or COS-7 cells, STIMATE did not seem to globally translocate to ER–PM junctions as STIM1 did after store depletion (Fig. 2f, Supplementary Fig. 3 and Supplementary Fig. 4a). However, when STIMATE was coexpressed with STIM1 in the same cell, we observed the co-localization of STIMATE with STIM1 at ER–PM junctions in a fraction of cells after store depletion. This phenomenon was less obvious under the confocal microscope but more pronounced when cells were examined by TIRF microscopy, which reports exclusively on fluorescence within 200 nm above the coverslip (Fig. 2g and Supplementary Fig. 4b). The coexpression of ORAI1 did not seem to increase the degree or tendency of STIMATE to co-localize with STIM1 (Supplementary Fig. 4c,d). Thus, a portion of STIMATE might translocate to ER–PM junctions in a STIM1-dependent manner in store-depleted cells. Together, our data imply that STIMATE co-localizes with STIM1 within the ER and might also reside in close proximity to STIM1 at ER–PM junctions in response to store depletion in mammalian cells.

After expression of mCherry–STIMATE in HEK293 cells co-transfected with STIM1, we frequently observed the spontaneous formation of STIM1 puncta even when the ER store was not depleted (Fig. 2g and Supplementary Fig. 4b,c). This scenario was most prominently visualized in cells stably expressing both ORAI1–CFP and STIM1–YFP (Fig. 3a–c). STIM1 puncta could be readily detected in cells transfected with mCherry–STIMATE before store

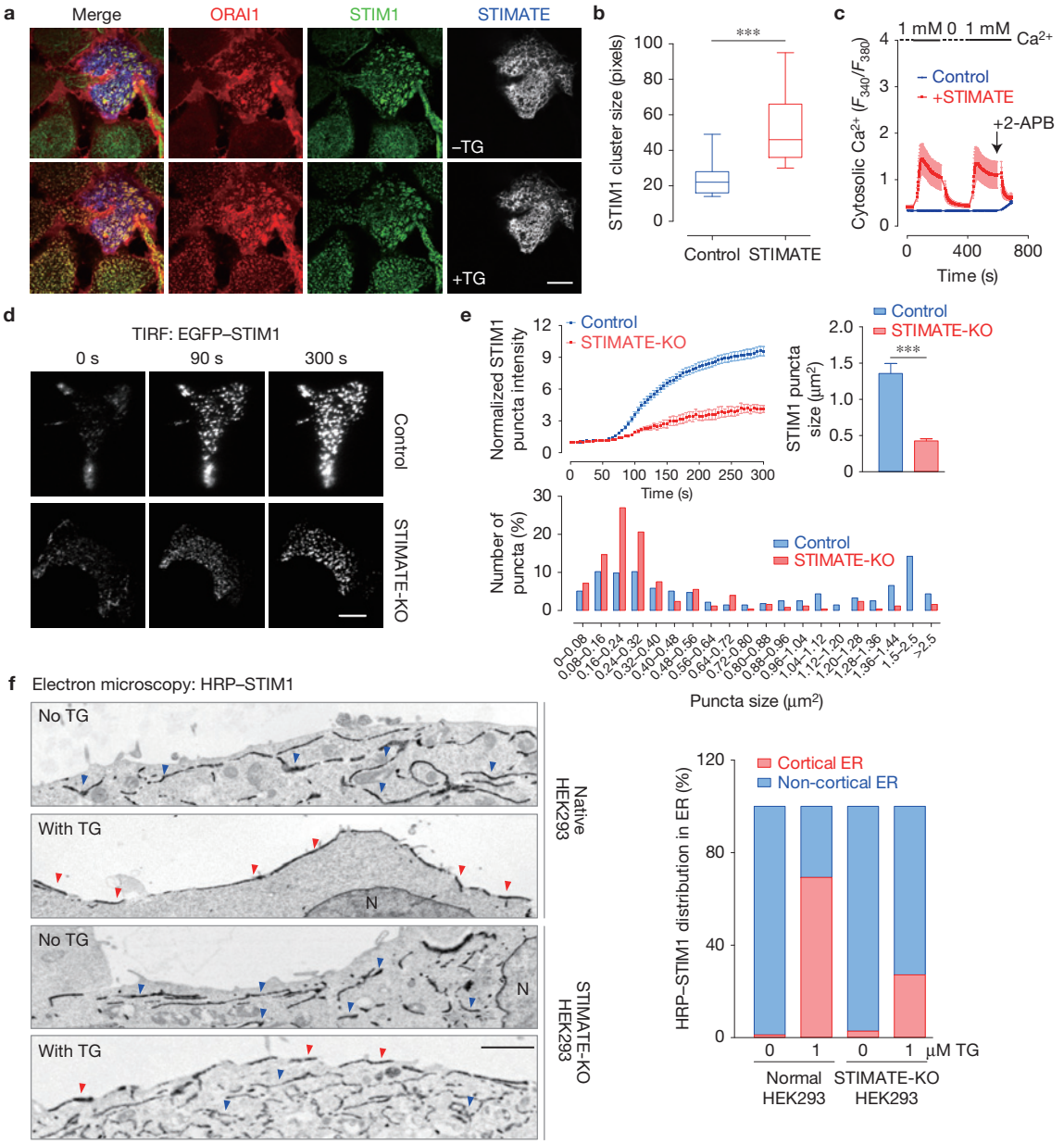

Figure 3 STIMATE facilitates efficient formation of STIM1 puncta at ER–PM junctions. (**a**) Confocal images at the footprint of STIM1–YFP + ORAI1–CFP HEK293 stable cells transiently transfected with mCherry–STIMATE. STIM1, ORAI1 and STIMATE are artificially coloured in green, red and grey, respectively, to aid visualization. Store depletion was triggered by 1 μm thapsigargin (TG). Scale bar, 10 μm. (**b**) Quantification of STIM1 cluster size in thapsigargin-stimulated cells treated as in **a**. The rectangle in the box plot shows the distribution of data between the first and third quartiles. The segment inside the rectangle shows the median, whereas the whiskers above and below the box mark the minimum and maximum. $^{***}P<0.001$ ($n=15$ cells pooled across three independent experiments; paired Student's *t*-test). (**c**) Constitutive Ca^{2+} influx elicited by transient expression of STIMATE in STIM1–YFP + ORAI1–CFP HEK293 stable cells. Ca^{2+} influx was inhibited by washing away external Ca^{2+} or by the addition of 50 μm 2-APB. Error bars denote s.e.m. for $n=15$ (control) or $n=20$ (STIMATE group) cells pooled across three independent experiments. (**d**) Representative TIRF images of STIM1 acquired 0, 90 or 300 s after depletion of ER Ca^{2+} stores with 1 μm thapsigargin in normal or STIMATE-KO HEK293 stable cells. Scale bar, 10 μm. (**e**) Time course of EGFP–STIM1 puncta formation (upper left panel) and quantification of STIM1 puncta size (upper right panel) and their distribution profiles (lower panel). Store depletion was induced by 1 μm thapsigargin. $^{***}P<0.001$ (compared with control; paired Student's *t*-test). Error bars denote s.e.m. for $n=6$ cells pooled across three independent experiments. (**f**) Electron micrographs of HRP–STIM1 in normal or STIMATE-KO HEK293 cells before and after store depletion triggered by 1 μm thapsigargin. Blue arrowheads, HRP–STIM1 staining in non-cortical intracellular ER pools; red arrowheads, HRP–STIM1 distribution at cortical ER that is separated <20 nm from PM. The bar graph on the right represents the quantification of HRP–STIM1 distribution in different pools of the ER (average of 5–10 cells). Scale bar, 2,000 nm. N, nucleus.

depletion. In contrast, the other cells in the same field without STIMATE overexpression showed an even distribution of STIM1 at the footprint of HEK293 cells (Fig. 3a). On store depletion, STIMATE-expressing cells formed significantly larger STIM1 puncta (Fig. 3b). Consistent with the pre-formation of STIM1 puncta before store depletion, overexpression of mCherry–STIMATE also elicited

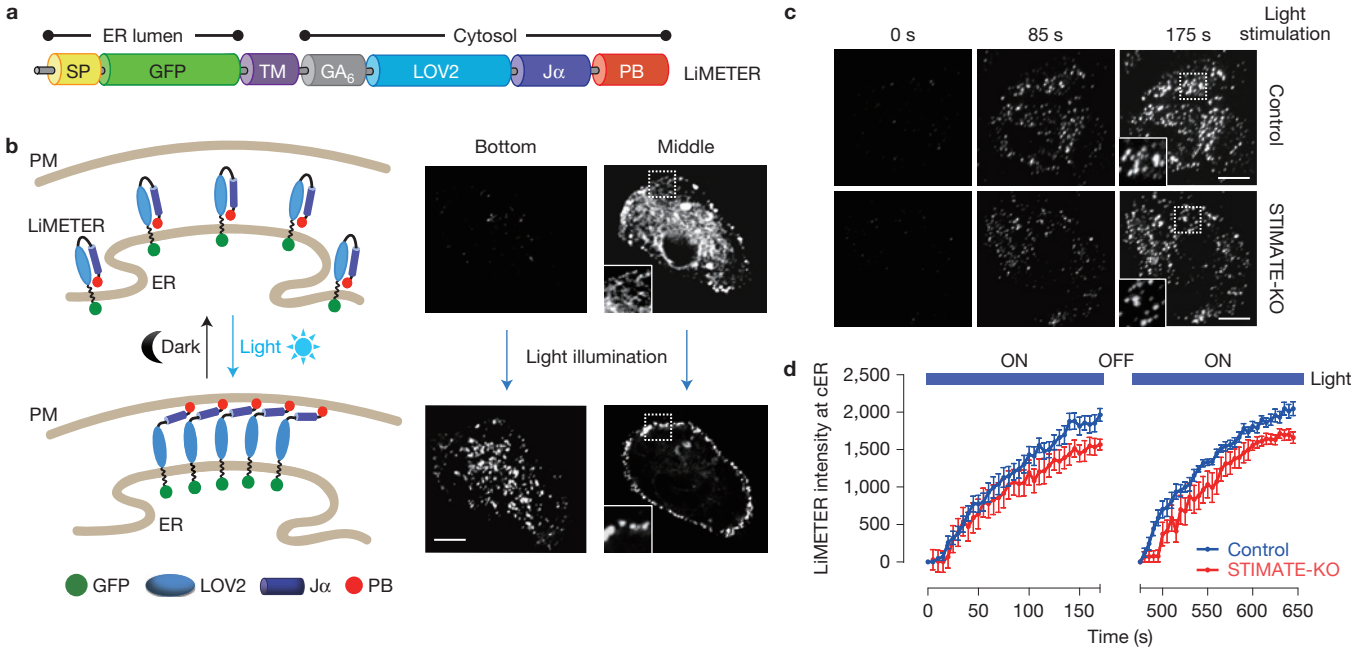

Figure 4 Effect of STIMATE depletion on cER accumulation reported by LiMETER. (**a**) Design of LiMETER as an optogenetic tool to photomanipulate ER–PM junctions and reversibly label cER. The ER luminal region of LiMETER includes a signal peptide (SP) and the single transmembrane domain (TM) derived from human STIM1, with GFP inserted in between as a reporter. The cytoplasmic region is composed of a $(GA)_6$ linker, the lightswitch LOV2 domain and a PM-targeting polybasic tail (PB) derived from the small GTPase Rit. (**b**) In the dark, the LOV2 Jα helix keeps the polybasic C-tail caged to prevent its targeting towards PM. LiMETER appears as a typical ER-resident protein like STIM1 at its resting state. On blue light stimulation (450–490 nm), the unwinding of the Jα helix exposes the PB domain to associate with phosphoinositides enriched in the inner leaflet of the plasma membrane, thereby promoting the formation of LiMETER puncta at cER (much as STIM1 forms puncta at ER–PM junctions). The confocal images on the right are representative confocal sections at the footprint or the middle layers of a typical LiMETER-expressing HEK293 cell before (upper) and after photoactivation (lower). A 488-nm laser was used as the light source to activate LiMETER while acquiring the GFP signals. Scale bar, 10 μm. (**c**,**d**) Representative TIRF images (**c**) and time course (**d**) of LiMETER accumulation at cER in response to light stimulation (488 nm with an estimated power density of 50 mW cm^{-2}) in normal (upper) or STIMATE-KO HEK293 cells (lower). For points falling within the time window of 125–175 s or 600–650 s, the difference of signal between control and STIMATE-KO was statistically significant ($P < 0.05$). Nonetheless, no significant difference was observed in the rate of LiMETER translocation towards cER ($P = 0.07$, paired Student's *t*-test). The LiMETER intensity was quantified using ImageJ software. Error bars denote s.e.m. for $n = 10$ (control) or $n = 12$ cells (STIMATE-KO) pooled across three independent experiment that emitted comparable total fluorescence signals under epifluorescence microscopy. Scale bar, 10 μm.

constitutive Ca^{2+} influx in these stably expressing cells when we switched the extracellular Ca^{2+} concentration from 0 to 1 mM (Fig. 3c). The Ca^{2+} flux could be reversed by withdrawing Ca^{2+} or by adding 2-APB, a pharmacological tool that is widely used at high concentrations (~50–100 μM) to block SOCE.

These findings led us to propose that STIMATE could modulate STIM1 puncta formation at ER–PM junctions. Indeed, genetic disruption of *STIMATE* in HEK293 (STIMATE-KO) cells induced a substantial reduction in the amounts of STIM1 puncta at ER–PM junctions (Fig. 3d and Supplementary Video 1). Compared with thapsigargin-stimulated normal HEK293 cells, the fluorescence intensity of EGFP–STIM1 at the TIRF layer of STIMATE-KO cells dropped by almost 70%. STIMATE knockout appreciably delayed the formation of STIM1 puncta, and resulted in a significant reduction in the puncta size at ER–PM junctions (Fig. 3e). An appreciable (~10–15%), but less pronounced, reduction in puncta formation was also observed in STIMATE-KO cells expressing the STIM1 gain-of-function mutants D76A and L258G (Supplementary Fig. 5a–d). Subsequent scrutiny under high-resolution electron microscopy further revealed that fewer STIM1 proteins migrated into cortical ER (cER, Fig. 3f and Supplementary Fig. 5e), a specialized ER network that lies immediately beneath the PM (<20 ~ 30 nm). In aggregate, these results indicate that STIMATE is required to promote efficient STIM1 clustering at ER–PM junctions, which might be achieved through modulating cER accumulation or modulating STIM1 activation as described below.

To examine the effect of STIMATE depletion on cER, we compared the cER accumulation in native and STIMATE-KO HEK293 cells. We used the genetically encoded fluorescent cER marker, MAPPER (membrane-attached peripheral ER), as readout because it has been recently shown to selectively label cER and co-localize tightly with activated STIM1 puncta at ER–PM junctions[20]. We noted that depletion of STIMATE caused approximately 8–10% decrease in the intensity or density of cER in HEK293 cells (Supplementary Fig. 5f–h). To rule out the possibility that the constitutive localization of MAPPER at ER–PM junctions might cause bias in our analysis on cER, we created an optogenetic tool, LiMETER (light-inducible membrane-tethered peripheral ER, Fig. 4 and Supplementary Video 2), to reversibly label cER. The ER luminal domain of LiMETER is composed of a signal peptide and the single transmembrane domain derived from STIM1, with GFP placed in between as a reporter. The cytoplasmic region of LiMETER contains a flexible linker and a genetically encoded lightswitch LOV2 domain (light oxygen voltage-sensing domain, residues 404–546)

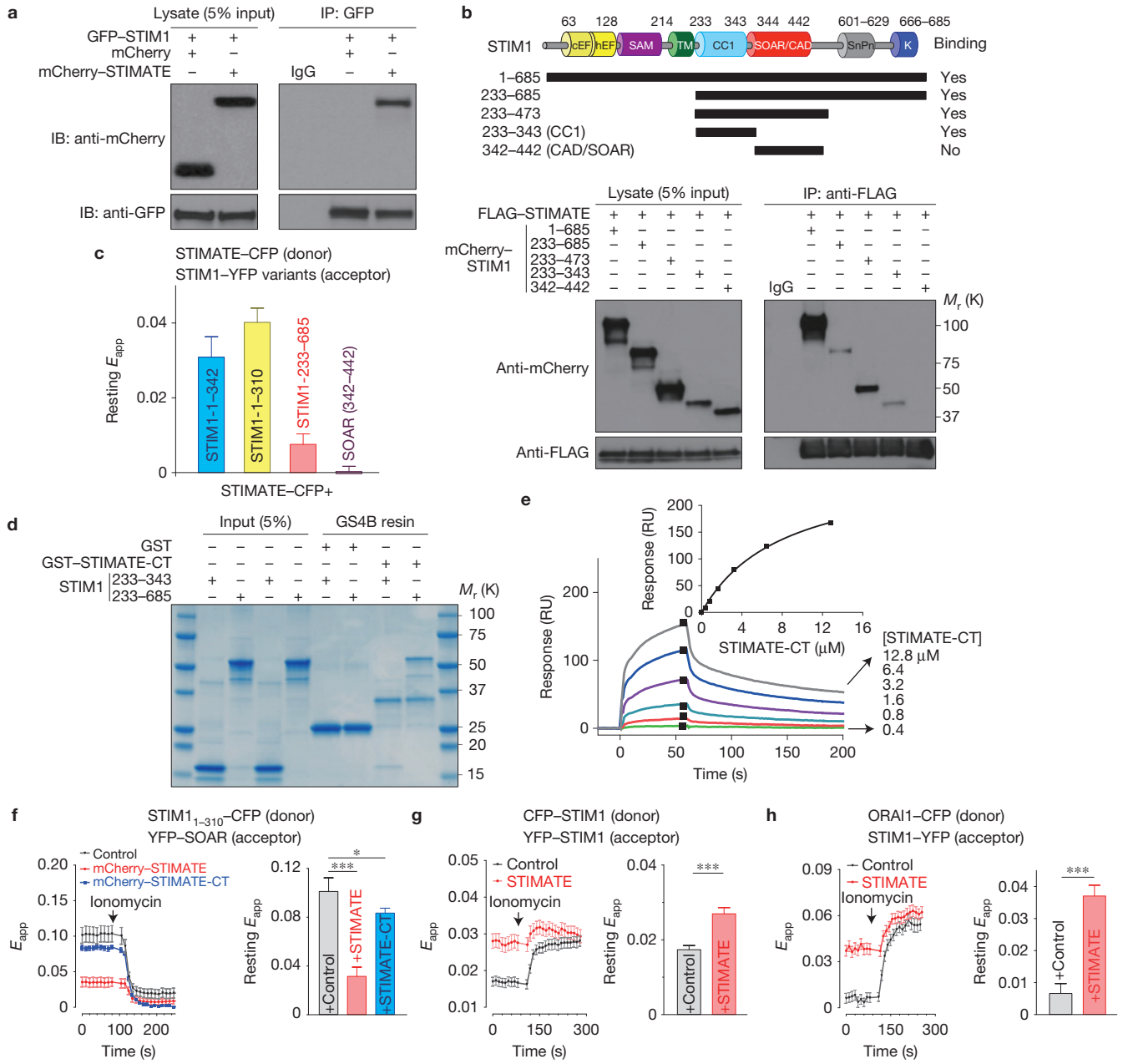

Figure 5 STIMATE interacts with STIM1 cytosolic fragments and promotes STIM1 conformational switch. (**a**) GFP–STIM1 coimmunoprecipitated with mCherry-tagged STIMATE but not mCherry (control). (**b**) FLAG–STIMATE coimmunoprecipitated with mCherry–STIM1 and the three indicated STIM1-CT fragments, but not with the minimal ORAI-activating domain CAD or SOAR. The domain architecture of STIM1 and design of truncated variants are shown at the top. (**c**) FRET signals measured in HEK293 cells co-transfected with the indicated donor–acceptor pairs without store depletion. YFP was C-terminally tagged to $STIM1_{1–342}$ and $STIM1_{1–310}$, and N-terminally fused with STIM1-CT (233–685) and SOAR or CAD. Error bars denote s.e.m. for $n=15$, 18, 20 or 17 cells, respectively (from left to right) pooled across three independent experiments. cEF, canonical EF-hand; hEF, hidden EF-hand; SAM, sterile alpha-motif; TM, transmembrane domain; CC1, coiled-coil region; SOAR/CAD, STIM-Orai activating region; SnPn, serine and proline-rich domain; K, polybasic C-tail. (**d**) *In vitro* binding of recombinant STIM1-CT and STIM1-CC1 to recombinant GST–STIMATE-CT proteins immobilized on glutathione (GS4B) resin. GST was used as a negative control. (**e**) Surface plasmon resonance measurements of the interaction between STIM1-CC1 and STIMATE-CT *in vitro*. Sensorgrams monitor the binding of STIMATE-CT (with concentrations labelled on the right) to immobilized STIM1-CC1 (with an N-terminal CGG linker to aid thiol coupling to the CM3 sensor chip). Inset: the peak values for each sensorgram were collected and a dose–response binding isotherm was created to obtain an apparent dissociation constant of 8.9 μm. One set of data representing three reproducible, independent experiments is shown. (**f**) FRET signals between $STIM1_{1–310}$–CFP (donor) and YFP–SOAR (acceptor) in HEK293 cells coexpressing mCherry (control black, $n=20$), mCherry–STIMATE (red, $n=24$) or mCherry–STIMATE-CT (blue, $n=30$ cells pooled across three independent experiments). Ionomycin (2.5 μm) was added to deplete ER Ca^{2+} stores. Left, time course. Right, bar graph of resting FRET signals $^{*}P<0.05$; $^{***}P<0.01$ (paired Student's *t*-test). Error bars denote s.e.m. (**g**,**h**) FRET signals in HEK293 cells stably expressing the indicated donor–acceptor pairs and transiently transfected with mCherry (control, black) or mCherry–STIMATE (red). The time course is shown on the left whereas the quantification of resting FRET signals is plotted to the right. $n=12$ cells for **g**; $n=15$ (control) or $n=20$ (STIMATE) cells pooled across three independent experiments for **h**. $^{***}P<0.01$ (paired Student's *t*-test). Error bars denote s.e.m. Unprocessed original scans of blots/gels are shown in Supplementary Fig. 6.

derived from *Avena sativa* phototropin 1 (refs 26,27), followed by a C-terminal PM-targeting polybasic tail isolated from the small G protein Rit[28] (Fig. 4a). In the dark, the Jα helix docks to the LOV2 domain and cages the polybasic tail to prevent its interaction with negatively charged PM-resident phosphoinositides. On blue light stimulation, photoexcitation generates a covalent adduct between a cysteine residue (Cys 450) and the flavin cofactor in LOV2, and subsequently promotes the undocking and unwinding of the Jα helix[26,27], thereby exposing the Rit polybasic C-tail to enable translocation of the protein towards PM to form puncta-like structures[28]. As a result, LiMETER underwent photo-inducible accumulation at ER–PM junctions to specifically label cER (Fig. 4 and Supplementary Video 2). Notably, this process can be reversibly repeated with multiple light–dark cycles without significant loss in the magnitude of response (Fig. 4d). This unique tool enables us to quantitatively examine the effect of STIMATE depletion on the dynamics of cER accumulation at defined spatiotemporal resolution. When compared with native HEK293 cells, we observed 10–12% decrease in the rate and extent of LiMETER accumulation at ER–PM junctions in STIMATE-KO HEK293 cells after blue light illumination (Fig. 4c,d). Thus, by using either MAPPER or LiMETER as a cER marker, we found that genetic depletion of STIMATE noticeably affects cER accumulation in HEK293 cells. Nonetheless, the ∼10% decrease in the efficiency of cER accumulation could not fully explain the more pronounced effect (∼70%) on STIM1 puncta formation in STIMATE-depleted cells (Fig. 3d,e). This prompted us to further explore alternative mechanisms by focusing on the initial activation steps of STIM1.

Results from both the BiFc (Supplementary Fig. 1a–c) and FRET (Fig. 2e) assays suggest a possible interaction between STIMATE and STIM1 in HEK293 cells. We further confirmed this by using coimmunoprecipitation (Fig. 5a). To investigate how STIMATE modulates STIM1 actions, we applied a combination of coimmunoprecipitation (Fig. 5b) and FRET (Fig. 5c) methods to map the domain(s) within STIM1 that mediate its interaction with STIMATE. We narrowed down the minimal STIMATE-interacting domain to the juxtamembrane coiled coil region of STIM1 (STIM1-CC1, residues 233–343). In both assays, the minimal ORAI-activating domain of STIM1 (CAD/SOAR; refs 29,30) showed negligible or no discernible interaction with STIMATE. As the longest cytosolic fragment of STIMATE protein is its C-terminal region (STIMATE-CT, residues 214–294, Fig. 2a and Supplementary Fig. 1d), we further expressed STIMATE-CT in bacteria and purified the recombinant protein to examine whether it would directly interact with STIM1 cytosolic domains. GST-tagged STIMATE-CT immobilized on GS4B resin was able to pull down both the entire STIM1 cytoplasmic domain (233–685) and STIM1-CC1 (Fig. 5d). The dissociation constant of the interaction between STIMATE-CT and STIM1-CC1 was further determined to be 8.9 ± 0.7 μM (Fig. 5e). Overall, these studies clearly demonstrated a direct physical contact between STIMATE and STIM1 *in vitro*.

After store depletion, STIM1 is activated through a conformational switch mechanism by undocking CAD/SOAR from CC1, thus projecting CAD/SOAR towards the PM to engage and gate ORAI1 channels[31]. The observation of a direct interaction between STIMATE-CT and STIM1-CC1 raised the possibility that STIMATE might promote STIM1 conformational switch through disrupting the intramolecular trapping mediated by CC1–SOAR association[32]. To test this, we developed a two-component FRET assay by fusing CFP or YFP to $STIM1_{1–310}$ and SOAR, respectively. This assay enabled us to monitor CC1–SOAR interaction in real time, and more importantly, to examine the effect of STIMATE on the STIM1 conformational switch in living cells[32]. Under resting conditions, YFP–SOAR was tightly docked towards the ER-resident $STIM1_{1–310}$ and showed a high resting FRET signal (Fig. 5f). On ionomycin stimulation, YFP–SOAR undocked from CC1 and thus caused a profound decrease of the FRET signal. The coexpression of STIMATE in this assay significantly reduced the resting FRET signal (Fig. 5f), implying that STIMATE could at least partially release STIM1 autoinhibition possibly by weakening CC1–SOAR association at rest. STIMATE-CT exhibited a similar effect but was much less potent, probably because this process requires anchoring of the STIMATE C-tail in the vicinity of the ER membrane or it involves coordinated actions of the C-tail with other regions of STIMATE. The consequence of STIMATE-mediated action on STIM1 was further reflected in enhanced FRET signals between CFP–STIM1 and YFP–STIM1 (Fig. 5g) or STIM1–YFP and ORAI1–CFP at rest (Fig. 5h), and culminated in constitutive Ca^{2+} influx (Fig. 3c). Clearly, our data provide compelling evidence to support a model in which STIMATE interacts with the juxtamembrane CC1 region of STIM1 to perturb the CC1–SOAR association that is the basis for STIM1 autoinhibition[32], thereby shifting the equilibrium towards activated states to promote the conformational switch and subsequent translocation of STIM1 towards ER–PM junctions.

In summary, we have applied a non-disruptive biotin labelling approach to capture protein complexes in close proximity to STIM1 at ER–PM junctions in living cells. Our findings not only afford an initial view on the protein composition of intact ER–PM junctions under physiological conditions, but also provide a framework for future dissection of their roles in cellular signalling, human health and disease. In particular, our study has established an irreplaceable role of the previously unrecognized ER-resident protein STIMATE in modulating STIM1-dependent Ca^{2+} signalling at ER–PM junctions. Major questions that warrant further investigation include: how STIMATE choreographs with other components at ER–PM junctions to coordinate Ca^{2+} signalling and other cellular events; and how STIMATE itself contributes to the formation and maintenance of ER–PM junctions. □

METHODS

Methods and any associated references are available in the online version of the paper.

Note: Supplementary Information is available in the online version of the paper

ACKNOWLEDGEMENTS

We are grateful to R. Lewis at Stanford University for the HRP–STIM1, mCherry–STIM1, and mCherry–CAD constructs. We thank J. Liou at University of Texas Southwestern Medical Center for sharing with us the MAPPERs construct, and Z. Songyang at Baylor College of Medicine for the BiFc-related constructs. We thank M. Höök at Texas A&M University for access to the Biacore 3000, D. Liu at Baylor College of Medicine for access to the Cell Based Assay Screening Facility and advice on BiFc, and R. Payne at Texas A&M University for technical support in electron microscopy studies. This work was supported by National Institutes of Health grants (R01 GM112003 to Y.Z., R01 AI084167, R01 CA143811 to C.L.W., and R01 GM110397 to P.G.H.), a Special Fellow Award from the Leukemia & Lymphoma Society (LLS 3013-12 to Y.Z.), a Robert A. Welch Endowed Chair in Chemistry (BE-0023) to C.L.W., the China Scholarship Council (to J.J.), the National Natural Science Foundation of China (NSFC31471279 to Y.W. and NSFC-81222020 to L.C.), the Recruitment Program for Young Professionals of China (to Y.W.),

the Program for New Century Excellent Talents in University (NCET-13-0061 to Y.W.), the American Heart Association SDG (13SDG17200006 to S.L.Z.), a Cancer Prevention Research Institute of Texas grant (to Y.H.), and by an allocation from the Texas A&M University Health Science Center Startup Fund (to Y.Z.).

AUTHOR CONTRIBUTIONS

Y.Z. and Y.W. supervised and coordinated the study. L.H., J.J., A.Q. and Y.Z. designed and generated all the plasmid constructs. L.H. performed the BiFc assays. J.J., P.T. and L.H. generated the knockout cell lines. L.H., Y.D. and M.-Q.D. prepared the proteomic samples and performed the mass spectrometry analyses. G.M., J.J., X.L. and Y.Z. developed the *in vitro* assays, and carried out the experiments with assistance from L.H., P.T. and Y.H. A.S., J.J., Y.W. and S.L.Z. performed the Ca^{2+} influx assay. J.J., A.S., A.Q., L.H., X.Z., L.C., L.Z. and Y.W. performed all the fluorescence imaging and other cell-based experiments. X.S. contributed to the synthesis of biotin–phenol. Y.Z., J.J., Y.D., L.H., A.S., G.M., Y.W. and M.-Q.D. analysed data, with input from the other authors. P.G.H., Y.H. and C.L.W. provided intellectual inputs to the manuscript. J.J., Y.W. and Y.Z. wrote the manuscript.

COMPETING FINANCIAL INTERESTS

The authors declare no competing financial interests.

Published online at http://dx.doi.org/10.1038/ncb3234
Reprints and permissions information is available online at www.nature.com/reprints

1. Carrasco, S. & Meyer, T. STIM proteins and the endoplasmic reticulum-plasma membrane junctions. *Annu. Rev. Biochem.* **80,** 973–1000 (2011).
2. Elbaz, Y. & Schuldiner, M. Staying in touch: the molecular era of organelle contact sites. *Trends Biochem. Sci.* **36,** 616–623 (2011).
3. Hogan, P. G., Lewis, R. S. & Rao, A. Molecular basis of calcium signaling in lymphocytes: STIM and ORAI. *Annu. Rev. Immunol.* **28,** 491–533 (2010).
4. Stefan, C. J., Manford, A. G. & Emr, S. D. ER-PM connections: sites of information transfer and inter-organelle communication. *Curr. Opin. Cell Biol.* **25,** 434–442 (2013).
5. Rhee, H. W. *et al.* Proteomic mapping of mitochondria in living cells via spatially restricted enzymatic tagging. *Science* **339,** 1328–1331 (2013).
6. Lam, S. S. *et al.* Directed evolution of APEX2 for electron microscopy and proximity labeling. *Nat. Methods* **12,** 51–54 (2015).
7. Kerppola, T. K. Bimolecular fluorescence complementation (BiFC) analysis as a probe of protein interactions in living cells. *Annu. Rev. Biophys.* **37,** 465–487 (2008).
8. Porter, K. R. & Palade, G. E. Studies on the endoplasmic reticulum. III. Its form and distribution in striated muscle cells. *J. Biophys. Biochem. Cytol.* **3,** 269–300 (1957).
9. Mayer, G. & Bendayan, M. Biotinyl-tyramide: a novel approach for electron microscopic immunocytochemistry. *J. Histochem. Cytochem.* **45,** 1449–1454 (1997).
10. Bendayan, M. Tech.Sight. Worth its weight in gold. *Science* **291,** 1363–1365 (2001).
11. Sharma, S. *et al.* An siRNA screen for NFAT activation identifies septins as coordinators of store-operated Ca^{2+} entry. *Nature* **499,** 238–242 (2013).
12. Min, S. W., Chang, W. P. & Sudhof, T. C. E-Syts, a family of membranous Ca^{2+}-sensor proteins with multiple C2 domains. *Proc. Natl Acad. Sci. USA* **104,** 3823–3828 (2007).
13. Manjarres, I. M., Rodriguez-Garcia, A., Alonso, M. T. & Garcia-Sancho, J. The sarco/endoplasmic reticulum Ca(2+) ATPase (SERCA) is the third element in capacitative calcium entry. *Cell Calcium* **47,** 412–418 (2010).
14. Wang, Y. *et al.* The calcium store sensor, STIM1, reciprocally controls Orai and CaV1.2 channels. *Science* **330,** 105–109 (2010).
15. Park, C. Y., Shcheglovitov, A. & Dolmetsch, R. The CRAC channel activator STIM1 binds and inhibits L-type voltage-gated calcium channels. *Science* **330,** 101–105 (2010).
16. Grigoriev, I. *et al.* STIM1 is a MT-plus-end-tracking protein involved in remodeling of the ER. *Curr. Biol.* **18,** 177–182 (2008).
17. Soboloff, J., Rothberg, B. S., Madesh, M. & Gill, D. L. STIM proteins: dynamic calcium signal transducers. *Nat. Rev. Mol. Cell Biol.* **13,** 549–565 (2012).
18. Giordano, F. *et al.* PI(4,5)P(2)-dependent and Ca(2+)-regulated ER-PM interactions mediated by the extended synaptotagmins. *Cell* **153,** 1494–1509 (2013).
19. Tabb, D. L., McDonald, W. H. & Yates, J. R. 3rd DTASelect and Contrast: tools for assembling and comparing protein identifications from shotgun proteomics. *J. Proteome Res.* **1,** 21–26 (2002).
20. Chang, C. L. *et al.* Feedback regulation of receptor-induced Ca^{2+} signaling mediated by E-Syt1 and Nir2 at endoplasmic reticulum-plasma membrane junctions. *Cell Rep.* **5,** 813–825 (2013).
21. Maleth, J., Choi, S., Muallem, S. & Ahuja, M. Translocation between PI(4,5)P2-poor and PI(4,5)P2-rich microdomains during store depletion determines STIM1 conformation and Orai1 gating. *Nat. Commun.* **5,** 5843 (2014).
22. Cong, L. *et al.* Multiplex genome engineering using CRISPR/Cas systems. *Science* **339,** 819–823 (2013).
23. Zurek, N., Sparks, L. & Voeltz, G. Reticulon short hairpin transmembrane domains are used to shape ER tubules. *Traffic* **12,** 28–41 (2011).
24. Russ, W. P. & Engelman, D. M. The GxxxG motif: a framework for transmembrane helix–helix association. *J. Mol. Biol.* **296,** 911–919 (2000).
25. Lorenz, H., Hailey, D. W., Wunder, C. & Lippincott-Schwartz, J. The fluorescence protease protection (FPP) assay to determine protein localization and membrane topology. *Nat. Protoc.* **1,** 276–279 (2006).
26. Wu, Y. I. *et al.* A genetically encoded photoactivatable Rac controls the motility of living cells. *Nature* **461,** 104–108 (2009).
27. Harper, S. M., Neil, L. C. & Gardner, K. H. Structural basis of a phototropin light switch. *Science* **301,** 1541–1544 (2003).
28. Heo, W. D. *et al.* PI(3,4,5)P3 and PI(4,5)P2 lipids target proteins with polybasic clusters to the plasma membrane. *Science* **314,** 1458–1461 (2006).
29. Park, C. Y. *et al.* STIM1 clusters and activates CRAC channels via direct binding of a cytosolic domain to Orai1. *Cell* **136,** 876–890 (2009).
30. Yuan, J. P. *et al.* SOAR and the polybasic STIM1 domains gate and regulate Orai channels. *Nat. Cell Biol.* **11,** 337–343 (2009).
31. Zhou, Y. *et al.* Initial activation of STIM1, the regulator of store-operated calcium entry. *Nat. Struct. Mol. Biol.* **20,** 973–981 (2013).
32. Ma, G. *et al.* Inside-out Ca^{2+} signaling prompted by STIM1 conformational switch. *Nat. Commun.* **6,** 7826 (2015).

DOI: 10.1038/ncb3234

METHODS

Chemicals. Tris(2-carboxyethyl)phosphine and disuccinimidyl suberate were obtained from Pierce. All other reagents were from Sigma Aldrich unless otherwise indicated. Biotin–phenol was initially obtained as a gift from A. Ting at Massachusetts Institute of Technology and later synthesized by following the reported synthesis scheme[5].

Antibodies. Streptavidin–DyLight594 (catalogue no. 21842, 1:2,000 for immunofluorescence staining) and streptavidin–HRP (N100, 1:4,000 for western blotting (WB)) were purchased from Thermo Scientific. Mouse monoclonal anti-FLAG antibody (clone number M2, catalogue no. F3165, 1:3,000 WB, 1.25 µg per 100 µg of total protein for immunoprecipitation (IP)) was purchased from Sigma. The rabbit polyclonal anti-GFP antibody (sc-8334, 1:1,000 WB, 0.5 µg per 100 µg of total protein for IP) was obtained from Santa Cruz Biotechnology. The mouse monoclonal and rabbit polyclonal anti-mCherry antibodies were obtained from Clontech (clone number 1C51, catalogue no. 632543, 1:1,000 WB) and Novus Biologicals (NBP2-25157, 1:2,000 WB), respectively. Mouse anti-rabbit IgG conformation specific (L27A9)-HRP (5127s, 1:2,000) antibody was obtained from Cell Signaling and used in IP experiments. Secondary antibodies, including goat anti-mouse IgG–HRP (sc-2005, 1:2,000) and goat anti-rabbit IgG-HRP (sc-2004, 1:2,000), were purchased from Santa Cruz Biotechnology.

Cell lines. Cell lines including HEK293 (CRL-1573), HeLa (CCL-2) and COS-7 (CRL-1651) were purchased from American Type Culture Collection (ATCC). The cell lines were validated by short tandem repeat profiling analysis by ATCC. Cells stably expressing STIM1, ORAI1 or STIM1–ORAI1 were subsequently generated on the basis of the aforementioned cell lines after geneticin or puromycin selection. All of the cell lines were free of mycoplasma contamination.

Plasmids. The cDNA clone encoding human STIMATE was purchased from DNASU Plasmid Repository. GFP–STIMATE, STIMATE–GFP and FLAG–STIMATE were generated through gateway cloning by using the vectors pCDNA-DEST54, pCDNA-DEST47 (Life Technologies), and a customized FLAG-tagged destination vector. STIMATE–YFP and STIMATE–CFP was made by inserting STIMATE between NheI–BamHI sites of pEYPF-N1 or pECFP-N1 (ClonTech). mCherry–STIMATE or CFP–STIMATE was made by inserting amplified fragments into the pCDNA3.1(+) vector. mCherry-tagged STIMATE truncation variants were made by ligation into pmCherry-N1 between NheI–BamHI sites. STIMATE mutant constructs were subsequently made by using the QuikChange Lightning Multi site-directed mutagenesis kit (Agilent). Full-length cDNA of human STIM1 was subcloned into pCMV6-XL5 (Origene)[33] with the insertion of EGFP or YFP between two additional NarI sites introduced immediately after residue Asn 38. For STIM1–YFP constructs, human STIM1 was inserted into pEYFP-N1 between XhoI and BamHI. pCDNA3.1(+)-mCherry-ORAI1 was made by sequential insertion of mCherry and human *ORAI1*. The ER labelling plasmid pDsRed2-ER was obtained from Clontech. mCherry–Sec61β, mCherry–STIM1 (ref. 29), STIM1–mOrange, YFP–SOAR (ref. 30), mCherry–CAD (ref. 29), ORAI1–YFP and HRP–STIM1 (ref. 33) were obtained from Addgene. The luciferase reporter pGL4.30[luc2P/NFAT-RE/Hygro] and the pRL-TK plasmid encoding *Renilla* luciferase were purchased from Promega. To generate EGFP–STIM1–APEX2 for *in situ* biotinylation, we replaced the mitochondria-targeting sequence with EGFP–STIM1 between the AflII–BamHI sites of pCDNA3-mito-APEX (Addgene: 42607) and further introduced the mutation A134P into the soybean APEX to enhance its enzymatic activity[5,6]. All of the constructs were confirmed by both DNA sequencing and diagnostic digestion.

Human STIM1–YFP_N was generated from pDONR221-STIM1 (DNASU) and pBabe-CMV-YFP_NDEST-neo[34] through Gateway cloning (Life Technologies). The prey library was generated by mixing pBabe-CMV-YFP_C-DEST-puro with Entry clones encoding selected candidate genes (obtained from DNASU, Supplementary Table 3) through Gateway cloning. To generate LiMETER, a human codon-optimized gBlock gene fragment was synthesized (Integrated DNA Technologies) based on the scaffold of MAPPERs (ref. 20) and cloned into pcDNA3.1(+) between NheI and XbaI sites, followed by replacing FRB with LOV2.

The sequences of STIM1 cytoplasmic fragments were amplified by PCR and cloned into the pProEX HTb vector (Life Technologies) between the BamHI and XhoI sites for expression as $(His)_6$-tagged proteins[31,35]. The STIMATE C-terminal domain (STIMATE-CT residues 214–294) was constructed as a fusion protein with the B1 domain of streptococcal protein G (GB1) for increased solubility or with glutathione *S*-transferase (GST) for pulldown assays. For the construct GB1–STIMATE-CT, we sequentially inserted GB1 at NcoI–BamHI sites and STIMATE-CT at BamHI–XhoI sites of the pProEx HTb vector. For the construct GST–STIMATE-CT, the gene was inserted into the pGEX-6P-1 vector at BamHI–EcoRI sites.

sgRNA-directed knockout of STIMATE using the CRISPR/Cas9 genome-editing tool. sgRNA targeting the sequence 5′-GGCATGCTGCTCATCTACGT GGGG-3′ (underscored, protospacer adjacent motif or PAM) on exon 4 of human *TMEM110* was designed with the online tool (http://crispr.mit.edu; ref. 22) and inserted into the BbsI site of the pSpCas9(BB)-2A-Puro vector (Addgene catalogue no. 48139) to generate px459-sgTMEM110. The sgRNA-containing plasmids were transfected into HEK293 cells and subjected to puromycin selection (2 µg ml^{-1}) for 2–4 days. Survival clones were then seeded into 96-well plates and later expanded to 24-well plates for maintenance in the presence of 1 µg ml^{-1} puromycin. The gene disruption was first confirmed by Surveyor nuclease assay (see below, Supplementary Fig. 2c) and ultimately validated by Sanger's sequencing (Supplementary Fig. 2d).

Surveyor nuclease assay for detection of genome modifications. Single colonies stably expressing px459-sgTMEM110 were picked up by using a limiting-dilution assay. Genomic DNA from control (transfected with empty pX459 vector) or STIMATE-KO stable cell clones was extracted using the Quick-gDNA Kit (Zymo Research). The genomic region flanking the CRISPR/Cas9 targeting site for *TMEM110* was PCR amplified by using the primers listed in Supplementary Table 4. The PCR products were purified using the Gel DNA Recovery Kit (Zymo Research) according to the manufacturer's instructions. Purified PCR products from control and stable cells were mixed and subjected to a reannealing process to produce heteroduplex formation by following the procedures described in the SURVEYOR Mutation Detection Kit (Transgenomic). After reannealing, products were treated with SURVEYOR nuclease and enhancer S (Transgenomic). The digested products were then subjected to electrophoresis on a 2% agarose gel and visualized with SYBR gold (Life Technologies) staining.

Quantitative real-time polymerase chain reaction (qPCR) analysis on STIMATE distribution. Total RNA was isolated from cells or tissues, and first-strand cDNA was generated from total RNA using oligo-dT primers and reverse transcriptase II (Life Technologies). Real-time qPCR was performed using specific primers and the ABI Prism 7000 analyser (Applied Biosystems) with the SYBR GreenER qPCR Super Mix Universal kit (Life Technologies). Target gene expression values were normalized to human *GAPDH* or mouse *Gapdh*. The primers used for qPCR were summarized in Supplementary Table 4.

Proteomic mapping of ER–PM junction in HEK293 cells. A step-by-step protocol describing GFP–STIM1–APEX2-mediated *in situ* biotinylation and further proteomic studies on ER–PM junctions can be found at *Nature Protocol Exchange* (http://dx.doi.org/10.1038/protex.2015.072).

Bimolecular fluorescence complementation assay and flow cytometry[34]. Ten thousand HEK293 cells seeded in 96-well plate were co-transfected with 50 ng µl^{-1} STIM1–YFP_N and prey–YFP_c using Lipofectamine 3000. Each condition was replicated in at least three wells. At 24 h post-transfection, cells were collected for high-throughput flow cytometric analysis on a LSRII flow cytometer equipped with a HTS sampler (BD Biosciences) through the Cell-Based Assay Screening Service core facility at Baylor College of Medicine. The percentage of YFP-positive cells was calculated by the software FlowJo.

Single-cell intracellular Ca^{2+} measurements. Intracellular [Ca^{2+}] was measured with Fura-2 AM as previously described[35–38]. In brief, HEK293 WT or STIM1–YFP/ORAI1–CFP stable cells were seeded and cultured on coverslips at least one day before imaging. To load Fura-2 AM, HEK293 cells were first kept in the imaging solution with 1 mM $CaCl_2$ and 2 µM Fura-2 AM for 30 min. Next, cells were kept in Fura-2 AM-free imaging solution with 1 mM $CaCl_2$ for another 30 min. For cells transfected with STIMATE that has constitutive Ca^{2+} influx, 300 µM Ca^{2+} or nominally Ca^{2+}-free solution was used to keep cells healthy. Emission fluorescence at 509 nm generated by 340-nm excitation light (F_{340}) and 380-nm light (F_{380}) was collected every two seconds, and intracellular Ca^{2+} levels are shown as the F_{340}/F_{380} ratio. After careful calibration, the Fura-2 intensities were further converted to Ca^{2+} concentrations as we routinely did in previous studies[35,37,39]. All experiments were carried out at room temperature. Traces shown are representative of at least three independent repeats with each including 15–60 single cells.

Fluorescence resonance energy transfer measurements. The same system used in Ca^{2+} measurements plus an Optosplit II Image Splitter (Cairn Research Limited) was used for FRET measurements. CFP ($428.9 \pm 5.5_{Ex}$/ $465 \pm 32_{Em}$), YFP ($502.6 \pm 11.2_{Ex}$/ $549 \pm 21_{Em}$), $FRET_{raw}$ ($428.9 \pm 5.5_{Ex}$/ $549 \pm 21_{Em}$) filters were used to capture raw images (F_{CFP} F_{YFP} and F_{raw}, respectively) every 10 s at room temperature. To generate apparent FRET efficiency, E_{app}, the following calculations on raw images were performed. First, three-channel-corrected FRET was calculated using the following formula: $FRET_c = F_{raw} - F_d/D_d^* F_{CFP} - F_a/D_a^* F_{YFP}$, where $FRET_c$ represents the corrected total amount of energy transfer, F_d/D_d represents measured bleed-through

of CFP into the FRET filter (0.84), and F_a/D_a represents measured bleed-through of YFP through the FRET filter (0.13). Second, to reduce variations caused by differences in expression levels, $FRET_c$ values were further normalized against donor fluorescence (F_{CFP}) to generate N-FRET (normalized FRET) signal. Third, E_{app} was calculated using the following equation: E_{app} = N-FRET/(N-FRET+G; ref. 40), where G (4.59) is the system-dependent factor[40]. A fluorescence probe, YFP–STIM1-D76G–CFP, was expressed in HEK293 cells to examine the relative expression level of CFP-tagged protein to YFP-tagged ones. This construct was used as a negative control in our FRET experiments because the donor (CFP) and the acceptor (YFP) were separated by ER membrane with a distance of >10 nm (ref. 1). To minimize fluctuations in E_{app} caused by variations of relative expression levels of donor protein to acceptor protein, only cells with a F_{CFP}/F_{YFP} ratio falling between 0.7 ∼ 1.4 were used for data analysis. All fluorescence images were collected and processed with MetaFluor software (Molecular Devices), and the resulting data were further analysed with Matlab R2012b software and plotted with Prism5 software. Representative traces of at least three independent experiments are shown as mean ± s.e.m.

NFAT-dependent luciferase assay. HEK293 cells were cultured in DMEM as described above in 24-well plates. After reaching 40–50% confluence, siRNA oligonucleotides were transfected using DharmaFECT (GE Dharmacon) for 48 h before further transfection of NFAT–luciferase reporter gene pGL4.30[luc2P/NFAT-RE/Hygro] (Promega). The *Renilla* luciferase gene (pRL-TK) was co-transfected as a control for counting transfected cells and normalizing the luminescence signals. HEK293 cells were treated with phorbol 12-myristate 13-acetate (PMA; 1 μM) and thapsigargin (1 μM) for 8 h. Three duplicates were used for each treatment. Cells were then collected and lysed by following the manufacturer's protocol. Luciferase activity was assayed using the Dual Luciferase Reporter Assay System (Promega) on a Biotek Synergy2 luminescence microplate reader. The ratio of firefly to *Renilla* luciferase activity was plotted for HEK293 cells. All of the data were normalized against the control group. For the rescue group, after 48 h treatment with siRNA, HEK293 cells were further transfected with the STIMATE-siRNA-resistant variant of mCherry–STIMATE, along with the NFAT–luciferase reporter genes and pRL-TK.

DSS-mediated crosslinking in HEK293 cells. HEK293 cells were plated in 6-well plates and maintained at 37 °C and 5% CO_2 for 24 h before transfection. After transient transfection with FLAG-tagged STIMATE, cells were washed three times with ice-cold PBS (pH 8.0) and treated with 0, 50, 100 and 250 μM of freshly prepared DSS. The mixture was incubated on ice for 1–5 min and the reaction was stopped by incubating the cells with a quenching solution containing 50 mM Tris-HCl at pH 8.0 for 15 min at room temperature. The cells were then lysed by lysis buffer (20 mM HEPES pH 7.4, 150 NaCl, 1 mM Na_2EDTA, 1 mM EGTA, 1% Triton, 2.5 mM sodium pyrophosphate and 1 mM β-glycerophosphate), mixed with an equal volume of 2× sample loading buffer, heated at 42 °C for 10 min (to avoid aggregation), and subjected to electrophoresis on 4–12% precast gel (Bio-Rad). After transferring the lysates to the polyvinylidene fluoride (PVDF) membrane, it was immunoblotted with a monoclonal mouse anti-FLAG M2 antibody (1:3,000, Sigma).

Confocal imaging and total internal reflection fluorescence (TIRF) microscopy. Cell lines used for imaging include HEK293, HeLa and COS-7 cells cultured on 35-mm glass-bottom dishes (MatTek) at 37 °C with 5% CO_2. All cells were grown in Dulbecco's modified Eagle's medium (DMEM, Sigma) supplemented with 10 mM HEPES, 100 units ml^{-1} penicillin, 100 μg ml^{-1} streptomycin and 10% heat-inactivated fetal bovine serum, unless otherwise noted. Confocal imaging was performed as previously described[32]. TIRF images were acquired on a NIKON Eclipse Ti-E microscope customized with Nikon A1R+ confocal laser sources with a ×60, NA 1.49 oil-immersion TIRF objective (Nikon). A 488-nm laser was used to excite GFP, and a 561-nm laser to excite mCherry. For two-colour imaging, 100-nm fluorescent beads (TetraSpecK Microspheres, Life Technologies) were deposited onto a coverslip and imaged as markers for later alignment.

To monitor LiMETER accumulation at ER–PM junctions, 50 ng LiMETER was transfected into normal or STIMATE-KO HEK293 cells using Lipofectamine 3000 (Life Technologies). Confocal images were acquired by using the Nikon A1R+ confocal laser sources. Images representative of the dark state of LiMETER (Fig. 4b with relatively low resolution) were acquired within 1 s using the fast scanning mode to minimize photoactivation of LiMETER by the 488-nm light source. TIRF time-lapse imaging of LiMETER was performed 24–36 h post-transfection. The 488-nm laser source used to acquire the GFP signal of LiMETER was applied to activate the photoswitch LOV2. The images were acquired every 5 s for 5 min as one cycle. The cells were then kept in the dark for 5–10 min, followed by subsequent cycles of photostimulation.

Electron microscopy. Normal or STIMATE-KO HEK293 cells were plated onto poly-L-lysine-coated chamber slides for electron microscopy. After transient transfection with HRP–STIM1, the cells were treated with or without 1–2 μm thapsigargin for 5 min in Ca^{2+}- and serum-free medium. The samples were washed with PBS twice and fixed using 2% glutaraldehyde in 0.1 M sodium cacodylate at room temperature for 1 h, then quickly moved to ice and washed with 0.1 M sodium cacodylate buffer for 10 min. HRP was visualized with 0.5 mg ml^{-1} diaminobenzidine and 0.03% hydrogen peroxide in 0.1 M sodium cacodylate buffer. Development of HRP took between 5 min and 20 min and was stopped by extensive washes with cold 0.1 M sodium cacodylate buffer. Cells were postfixed in 2% OsO_4 in 0.1 M cacodylate buffer (Electron Microscopy Sciences) at 4 °C for 1 h, washed in 0.1 M sodium cacodylate buffer and then contrasted in 2% aqueous uranyl acetate (Electron Microscopy Sciences) overnight at 4 °C, dehydrated in ethanol and embedded in epon for conventional electron microscopy. Images were acquired on a Morgagni transmission electron microscope (FEI) from Electron Microscopy Services provided by the Image Analysis Lab at Texas A&M University.

Image analyses. All acquired images were analysed using the NIKON NIS-Elements AR package or the ImageJ (NIH) software. The size of GFP–STIM1 puncta shown in Fig. 3b was quantified using ImageJ. Regions of interest (ROIs) within the images were determined using a manually selected pixel intensity threshold and the total pixel number per ROI was determined as a measure of puncta size. Using the same image analysis strategy, HRP–STIM1 relative distribution in ER was determined by measuring the total length of HRP-positive STIM1 segments and the length of multiple HRP-positive STIM1 segments migrated into cortical ER (separated within 20 nm from the PM). The Pearson correlation coefficient between EGFP–STIM1 and mCherry–STIMATE was calculated using the built-in co-localization analysis module of the NIS-Elements AR software. To determine the amount of MAPPER or LiMETER accumulation at cER and STIM1 puncta at ER–PM junctions, the TIRF images were background subtracted and converted to binary images to identify dim puncta and define the edges on the basis of optimized thresholds using the NIS-Elements AR software (Nikon).

Pulldown and coimmunoprecipitation experiments. Expression and purification of recombinant proteins, as well as GST pulldown assays, were carried out as we described previously[31,32,35]. Bound proteins were visualized on SDS–PAGE after Coomassie brilliant blue R-250 staining. For coimmunoprecipitation experiments, transfected HEK293 cells were washed in cold PBS 3 times and lysed directly using lysis buffer including 20 mM Tris-HCl (pH 7.5), 150 mM NaCl, 1 mM EDTA, 1 mM EGTA, 1% Triton X-100, 2.5 mM sodium pyrophosphate and 1 mM β-glycerophosphate, supplemented with protease inhibitor cocktail and phosphatase inhibitor cocktail (Sigma), for 30 min at 4 °C. The lysates were clarified by centrifugation at 20,000*g* at 4 °C for 15 min. Equivalent sample amounts were subjected to SDS–PAGE, followed by transferring to PVDF membranes and probing with the appropriate primary and HRP-conjugated secondary antibodies. For immunoprecipitation, the cell lysates were incubated with the indicated antibodies and magnetic A or G beads (Thermo Scientific) overnight at 4 °C. The beads were pelleted and washed with lysis buffer, in the presence of protease inhibitors 10 times and were then heated in SDS loading buffer for 10 min at 42 °C before resolving on SDS–PAGE. The cell lysates were separated by 4–15% gels (Bio-Rad), transferred to PVDF membranes and probed with the indicated antibodies.

BIAcore surface plasmon resonance (SPR) measurements. SPR-based Biacore experiments were performed at 25 °C on a Biacore 3000 instrument (GE Healthcare Bio-Sciences AB). The immobilized STIM1-CC1 sensor surface was prepared by ligand thiol coupling through the single cysteine residue at the N terminus of CGG-CC1 (ref. 31). The sensor chip CM3 and reagents for thiol coupling were purchased from GE Healthcare. The immobilization was performed at a 5 μl min^{-1} flow rate with PBS (10 mM sodium phosphate pH 7.4, 150 mM NaCl). The flow cell was activated by 0.4 M 1-ethyl-3-(3-dimethylaminopropyl)-carbodiimide and 0.1 M *N*-hydroxysuccinimide followed by washing with 80 mM of 2-(2-pyridinyldithio)ethylamine hydrochloride (GE Healthcare) in 0.1 M sodium borate (pH 8.5) to introduce reactive disulphide groups on the surface. Thirty microlitres of STIM1-CC1 (10 μg ml^{-1} in 10 mM sodium acetate pH 5.5) was injected to the activated surface and then blocked with 20 μl of cysteine/NaCl. Approximately 550 RU (response unit) of STIM1-CC1 was immobilized. A reference flow cell was prepared with the same activation and blocking steps but without any protein coupled. The binding study was performed at 50 μl min^{-1} flow rate using TBS (20 mM Tris, 150 mM NaCl, pH 7.5) as running buffer. After each injection of STIMATE-CT (twofold serial dilution in running buffer), the CC1 surface was regenerated by injecting 10 mM glycine (pH 1.7) for 30 s to remove bound STIMATE-CT. Background-corrected sensorgrams were collected for data analysis.

Statistical analyses. Unless otherwise noted, quantitative data are expressed as the mean and standard error of the mean (s.e.m.). Statistical significance was determined with paired Student's *t*-test. $^{*}P < 0.05$; $^{**}P < 0.01$; $^{***}P < 0.001$, when compared with control or WT.

DOI: 10.1038/ncb3234

33. Wu, M. M., Buchanan, J., Luik, R. M. & Lewis, R. S. Ca^{2+} store depletion causes STIM1 to accumulate in ER regions closely associated with the plasma membrane. *J. Cell Biol.* **174,** 803–813 (2006).
34. Lee, O. H. *et al.* Genome-wide YFP fluorescence complementation screen identifies new regulators for telomere signaling in human cells. *Mol. Cell. Proteom.* **10,** M110001628 (2011).
35. Zhou, Y. *et al.* STIM1 gates the store-operated calcium channel ORAI1 *in vitro*. *Nat. Struct. Mol. Biol.* **17,** 112–116 (2010).
36. Wang, Y. *et al.* STIM protein coupling in the activation of Orai channels. *Proc. Natl Acad. Sci. USA* **106,** 7391–7396 (2009).
37. Zhou, Y., Ramachandran, S., Oh-Hora, M., Rao, A. & Hogan, P. G. Pore architecture of the ORAI1 store-operated calcium channel. *Proc. Natl Acad. Sci. USA* **107,** 4896–4901 (2010).
38. Wang, X. *et al.* Distinct Orai-coupling domains in STIM1 and STIM2 define the Orai-activating site. *Nat. Commun.* **5,** 3183 (2014).
39. Zhang, S. L. *et al.* Genome-wide RNAi screen of Ca(2+) influx identifies genes that regulate Ca(2+) release-activated Ca(2+) channel activity. *Proc. Natl Acad. Sci. USA* **103,** 9357–9362 (2006).
40. Zal, T. & Gascoigne, N. R. Photobleaching-corrected FRET efficiency imaging of live cells. *Biophys. J.* **86,** 3923–3939 (2004).

nature cell biology

DOI: 10.1038/ncb3234

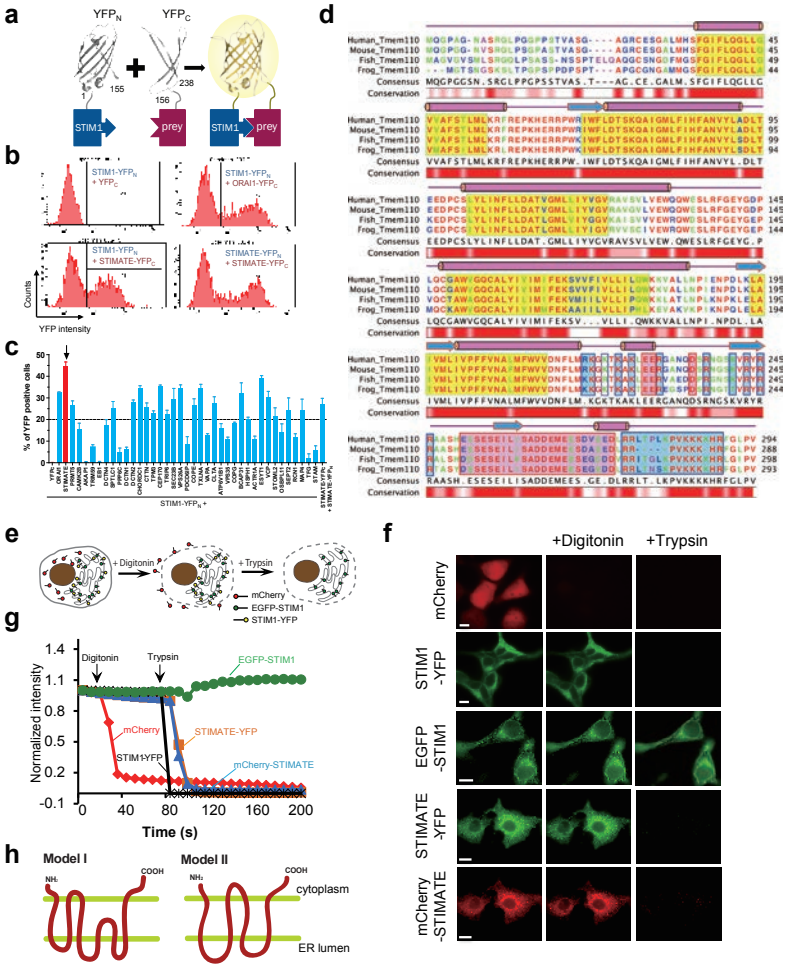

Supplementary Figure 1 BiFc assay as a secondary assay to validate STIM1 interactors and determination of STIMATE membrane topology (related to Figure 1). **a,** Scheme for the BiFc assay. The N-terminal portion of YFP (YFP$_N$, residues 1-155) is fused to the STIM1 C-terminus as the bait to prey against a customized library containing candidate genes fused with the C-terminal half of YFP (YFP$_C$, residues 156-238), or *vice versa*. STIM1 binding to its partners is anticipated to restore the YFP fluorescence. **b,** Representative examples of FACS profiles from the BiFc assays. STIM1-YFP$_N$ + YFP$_c$ was used a negative control, whilst STIMATE-YFP$_N$ + ORAI1-YFP$_C$ was used as positive control in the assay. In addition to strong YFP signals restored in HEK293 cells coexpressing STIM1-YFP$_N$ and a number of YFP$_C$-tagged genes, we also observed efficient recovery of YFP signals in cells coexpressing STIMATE-YFP$_N$ and STIMATE-YFP$_C$, implying the tendency of STIMATE to form oligomers. **c,** BiFc as a secondary assay to confirm selected STIM1 binding partners in HEK293T cells. YFP-positive cells were counted by FACS ad 20% was set as the threshold for strong positive hits. Store depletion was induced by 1-2 μM thapsigargin (TG), a widely-used inhibitor for SERCA pumps. For hits identified only under resting condition in the proteomic study (**Supplementary Table 1**), BiFc assay was performed without the addition of TG. Error bars represent s.e.m. from n=12 wells of cultured cells pooled across 3 independent experiments . Note that this set of data was also used in the scatter plot as X-axis in **Fig. 1d**. **d,** Multiple sequence alignment of the STIMATE (encoded by *TEMEM110*) proteins in vertebrates and the relative distribution of STIMATE mRNA in human and mouse tissues. The predicted TM segments were highlighted in yellow. Regions enriched with positively- or negatively residues in the STIMATE C-tail were boxed in blue or red, respectively. The secondary structure elements were displayed on the top of aligned primary sequences. Cylinder, α-helix; Arrow, β-strand. Sequence accession numbers in the Uniprot database are: human, Q86TL2; mouse, Q3UF25; fish, Q7SY08; frog, Q28EE1. **e-h,** Determination of STIMATE topology by the fluorescence protease protection (FPP) assay. **e,** Schematic representation of the FPP assay. Digitonin is added to HEK293 cells to permeabilize the plasma membrane and causes diffusion of cytosolic proteins outside the cell. The amount of digitonin is optimized to maintain the membrane integrity of ER. Subsequent addition of trypsin would cause the degradation of fluorescent protein tags exposed toward the cytosol (*e.g.*, STIM1-YFP, panel f), thus resulting in significant quenching of fluorescence. In contrast, the fluorescence tags residing within the subcellular organelles (*e.g.*, EGFP-STIM, panel f) remain intact and emit fluorescence. **f,** Confocal images of HEK293 cells expressing either N- or C-terminally FP tagged STIM1 or STIMATE or mCherry alone that were sequentially treated with digitonin and trypsin. Both fluorescence protein tagged constructs showed a pronounced reduction of fluorescence upon addition of trypsin, indicating that N and C-termini of STIMATE face the cytosolic side of ER. Note that STIMATE-YFP and mCherry-STIMATE were co-transfected into the same cells. **g,** Time course of fluorescence imaging following sequential addition of digitonin and trypsin. **h,** Cartoon depicting the tentative membrane topology of STIMATE. Computational prediction of membrane topology yielded two models. Most programs including TOPCONS, TMHMM and TMPred predicted five transmembrane segments in STIMATE. TM4 is predicted to contain ~30 amino acids (**Supplementary Fig. 1d**), a length that far exceeds the average length of typical integral membrane proteins of the ER (approximately 20 amino acids). It is likely that TM4 adopts a hairpin structure to penetrate but not span across the ER membrane, thus allowing both the N- and C-termini of STIMATE facing toward the same side. In model II, only four TM segments were predicted by the programs SCAMPI and SOSUI. The second TM segment in Model I was absent in Model II.

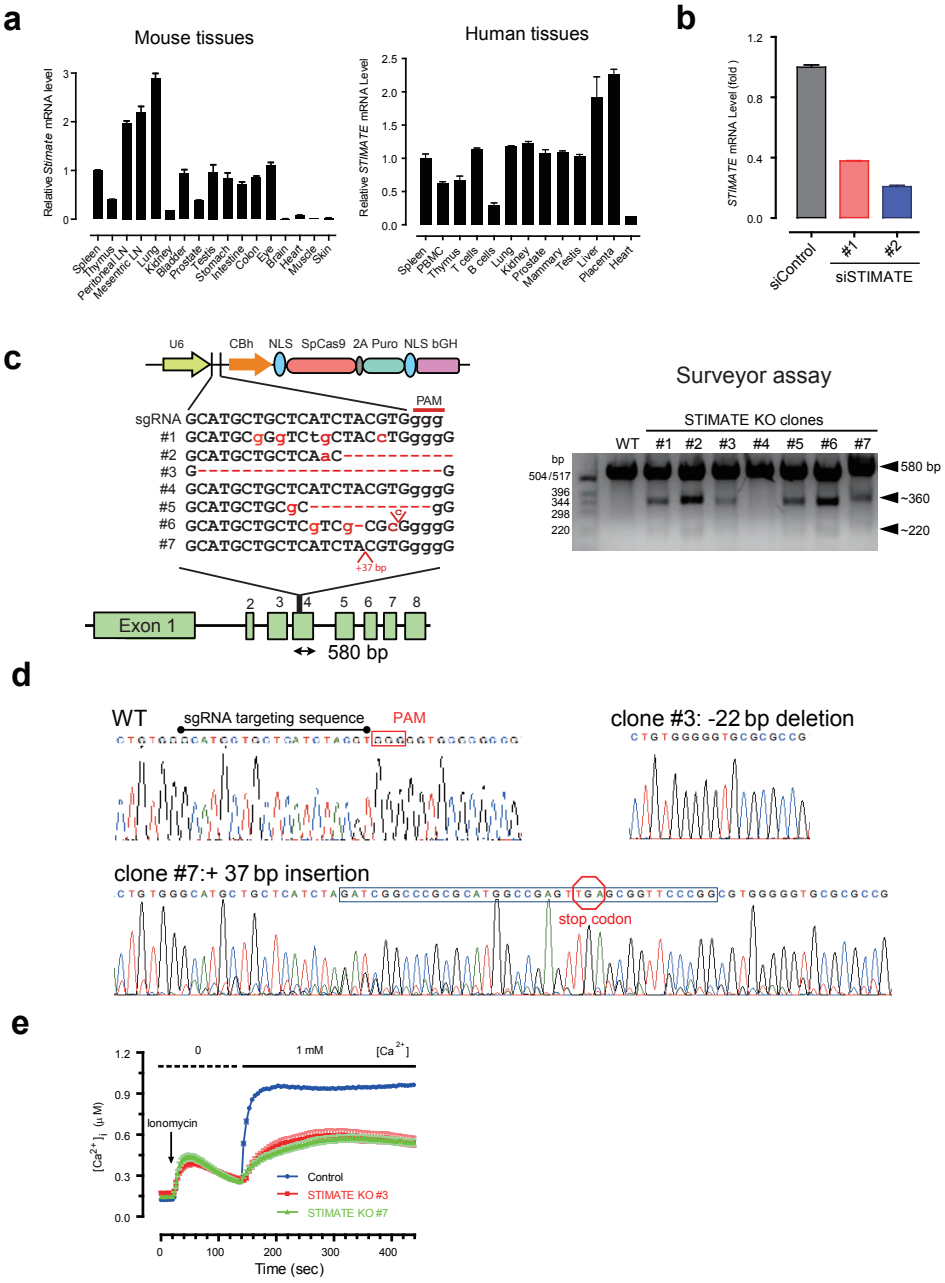

Supplementary Figure 2 Expression profiles of *STIMATE* and confirmation of *STIMATE* knockdown or knockout (related to Figures 1 and 3). **a,** mRNA expression profiles of STIMATE in mouse (left) and human (right) tissues (n=3 independent experiments). Data were plotted as average ± s.d.. **b,** Relative *STIMATE* mRNA levels in HEK293 cells transfected with indicated siRNA oligos. Error bars denote s.e.m. from n=3 independent experiments. **c,** Design of the guide sequence (sgRNA) to target the human *STIMATE* exon 4 for gene disruption by the Cas9 targeting vector pX459. Seven stable cell lines after puromycin selection were maintained and sequenced. Surveyor nuclease assay was further used to confirm gene disruption in stable clones after puromycin selection. **d,** Confirmation of gene disruption at *STIMATE* exon 4 with Sanger's sequencing. **e,** Ionomycin-induced Ca^{2+} flux in normal and STIMATE-KO HEK293 cells. Error bars represent s.e.m. from assays performed with n=30 (control), 36 (STIMATE KO#3), or 40 cells (STIMATE KO#7), respectively, pooled across three independent experiments.

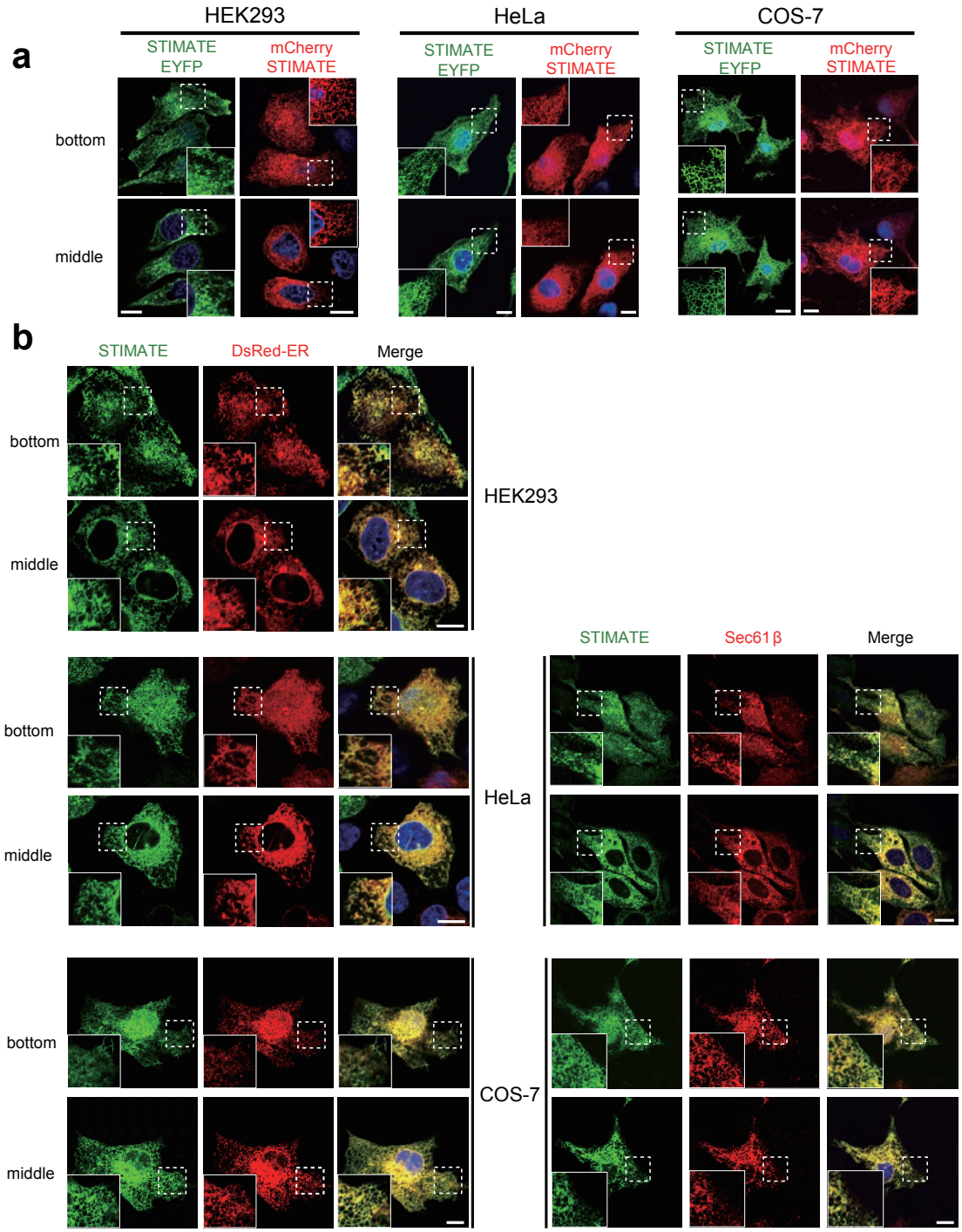

Supplementary Figure 3 Fluorescent protein (FP)-tagged STIMATE localizes to ER (related to Figures 2). **a,** Confocal images of HEK293, HeLa or COS-7 cells expressing STIMATE with FP tagged to its N- or C-terminus. Regardless of the position of FP tags, STIMATE displayed ER-like distribution. Blue, nuclear staining with Hoechst 33342. Scale bar, 10 μm. **b,** Colocalization of EGFP-STIMATE with ER marker proteins DsRed-ER or mCherry-Sec61β. Nuclei were stained in blue by Hoechst 33342. The insets show at higher magnification the regions outlined by dotted line. Scale bar, 10 μm.

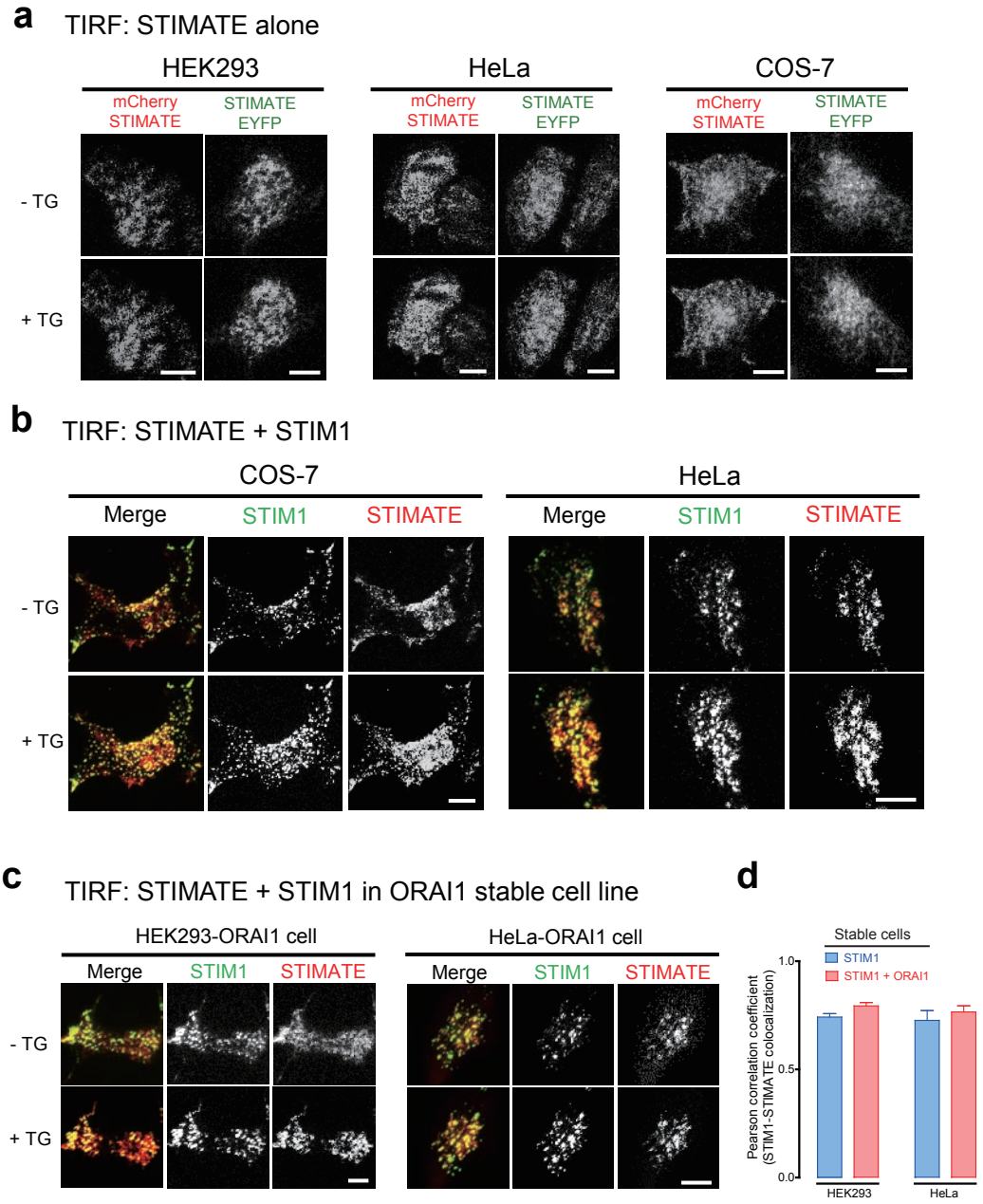

Supplementary Figure 4 TIRF imaging of STIMATE in indicated cells with or without coexpression of STIM1 or STIM1 + ORAI1 (related to Figures 2 and 3). 1 μM TG was added to induce store depletion. Scale bar, 10 μm. **a,** Representative TIRF images of HEK293, HeLa or COS-7 cells expressing STIMATE with mCherry tagged to its N-terminus or EYFP at its C-terminus. **b,** TIRF images of COS-7 or HeLa cells cotransfected with mCherry-STIMATE (red) and EGFP-STIM1 (green). **c**, TIRF images of EGFP-STIM1/ORAI1 stable cell lines transfected with mCherry-STIMATE. **d,** Quantification of STIM1-STIMATE colocalization by the Pearson correlation coefficient. mCherry-STIMATE was transfected into HEK293 or HeLa cells coexpressing STIM1 (blue) or STIM1 + ORAI1 (red) as illustrated in panels c-d. Error bars denote s.e.m. from n=6 (STIM1) or 10 (STIM1+ORAI1) cells pooled across two independent experiments.

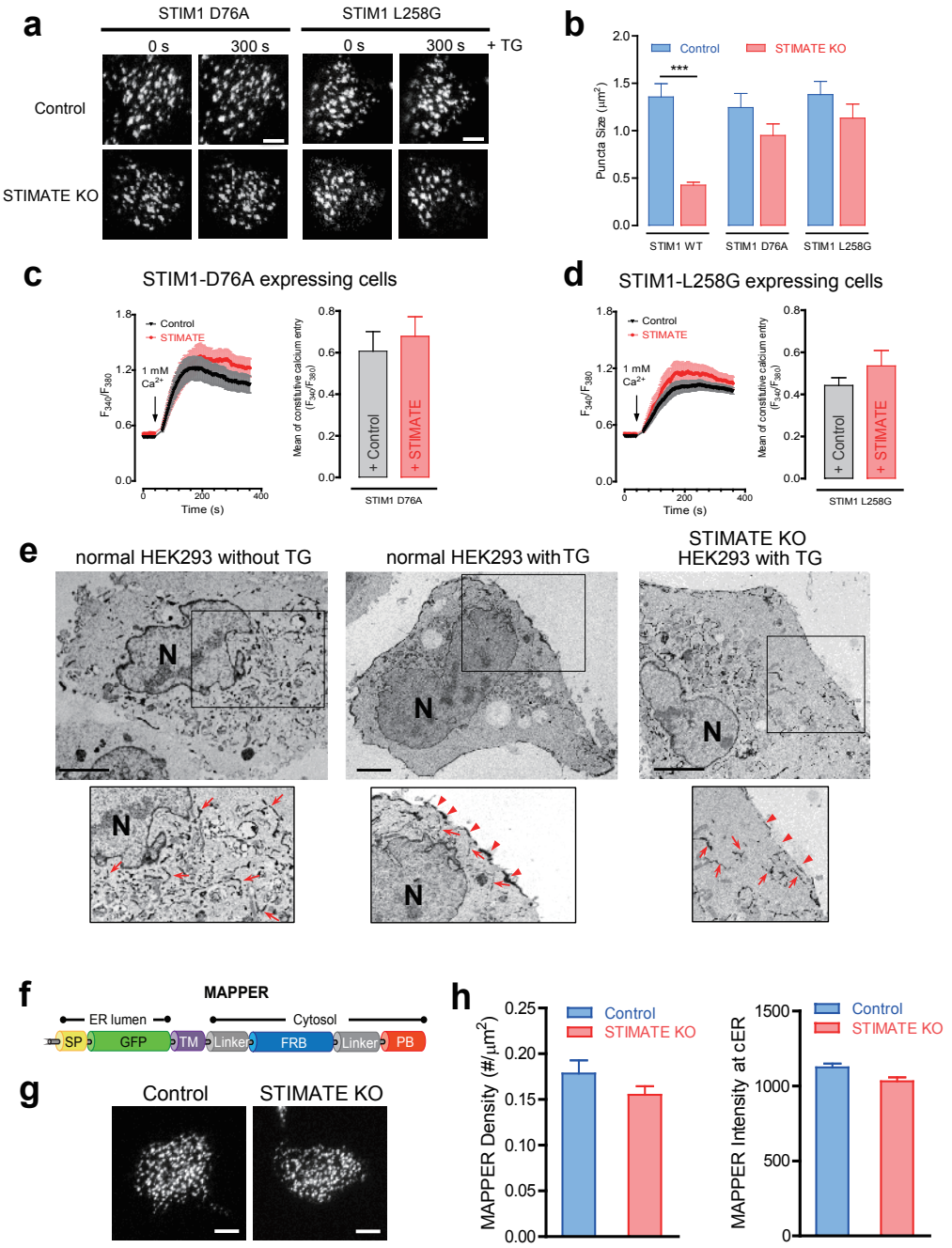

Supplementary Figure 5 Accumulation of STIM1 mutants or MAPPER at ER-PM junctions and representative examples of electron micrographs for HRP-STIM1 in normal or STIMATE-KO HEK293 cells (related to Figures 2 and 3). **a-d,** Effects of STIMATE depletion or overexpression on the action of STIM1 gain-of-function mutants. TIRF images (**a**) of EGFP-STIM1-D76A or EGFP-STIM1-L258G were acquired 0 or 300 seconds after store depletion induced by TG in normal or STIMATE-KO HEK293 cells. Scale bar, 10 μm. **b,** Quantification of puncta size of WT and mutant STIM1 in normal or STIMATE-KO HEK293 cells. Note that the data for WT STIM1 was also used in **Fig. 3e**. Error bars denote s.e.m. for n= 6 cells pooled across two independent experiments. ***P<0.001 (compared to control, paired student's *t*-test). **c-d,** Constitutive Ca^{2+} influx elicited by STIM1 gain-of-function mutant D76A (**c**) or L258G (**d**) in HE293 cells co-transfected with mCherry (control, black) or mCherry-STIMATE (red). Constitutive Ca^{2+} influx was monitored by Fura-2 when switching the external medium from 0 mM Ca^{2+} to 1 mM Ca^{2+}. Error bars denote s.e.m. from n=25 (control) and 28 (+ STIMATE) cells for D76A, or n= 30 (control) and 40 cells (+STIMATE) for L258G pooled across three independent experiments. **e.** Representative examples of EM images of HRP-STIM1 in normal or STIMATE-KO HEK293 cells. Compared to normal HEK293 cells, HRP-STIM1 exhibited less efficient translocation toward the ER-PM junction upon store depletion in STIMATE-KO cells. Arrowhead, HRP-STIM1 located at ER-PM junction; arrow, representative HRP-STIM1 staining in the cytosol (non-cortical ER regions). N stands for nucleus. Scale bar, 4000 nm. **f-h.** cER labeling by MAPPER in normal or STIMAT-KO HEK293 cells. **f,** Domain architecture of the genetically-encoded cER marker MAPPER. **g-h,** TIRF images (**g**) and quantification (**h**) of MAPPER accumulation at cER in control (empty vector) or STIMATE-KO HEK293 stable cells. Error bars denote s.e.m. for n=20 cells pooled across three independent experiments. Scale bar, 10 μm.

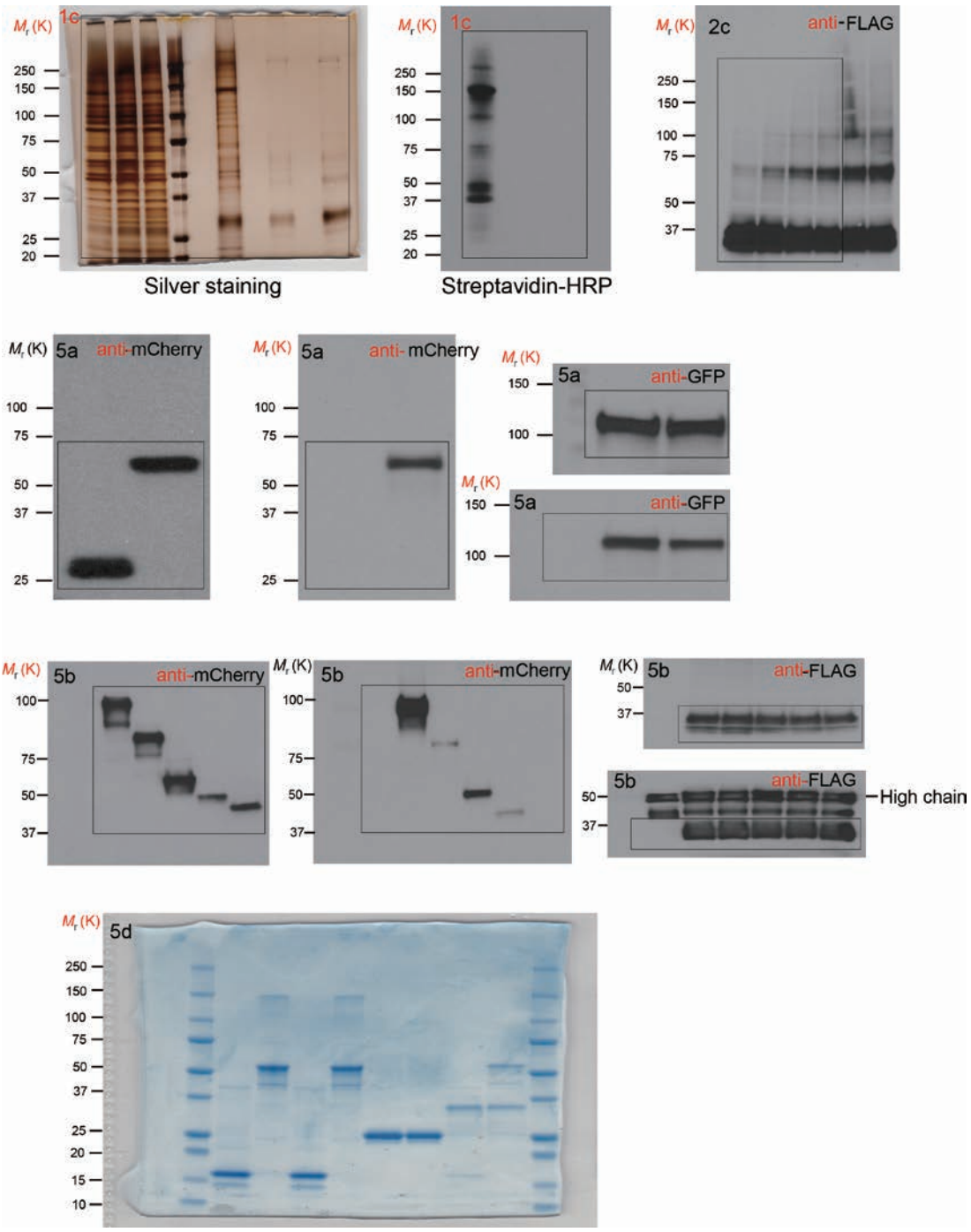

Supplementary Figure 6 Uncropped western blots or SDS-PAGE.

Supplementary Table 1. Top candidates emerged from proteomic mapping of protein complexes surrounding STIM1 via *in situ* APEX2-catalyzed biotin labeling before store depletion*.

UniProt ID	Gene Name	Spectral counts	Sequence coverage	Annotated/ reported functions & other remarks
ER-resident proteins				
Q13586	***STIM1***	***284***	***46.0%***	***Activator of ORAI channels; Positive hit from RNAi screening#***
Q86TL2	***TMEM110 (STIMATE)***	***22***	***21.4%***	***Multi-pass membrane protein; Positive hit from RNAi screening***
B4DGP8	CANX	15	20.9%	Calcium-binding protein assisting protein assembly; Binds STIM1
P30626	SRI	6	33.3%	Contains 4 EF-hand calcium-binding motifs; Modulates the activity of RyR2 calcium channels
H7C5W9	ATP2A2	5	8.0%	Sarcoplasmic/endoplasmic reticulum calcium ATPase 2; Binds STIM1
H0YL43	RCN2	3	26.5%	ER luminal calcium binding protein contains 6 EF-hands
H7C4H2	**SRPRB**	**3**	**20.6%**	**Component of the signal recognition particle receptor**
Posttranslational modifications (PTM) enzymes				
F5GZP3	***TRIM59***	***74***	***24.8%***	***Potential E3 ligase involved in ubiquitination; Positive hit from RNAi screening***
B4DV00	**PRMT5**	**7**	**4.4%**	**Arginine N-methyltransferase; PRMT depletion suppresses NFAT-dependent IL-2 production**
O15269	**SPTLC1**	**4**	**8.0%**	**ER-resident; involved in serine palmitoylation**
B7Z1Z6	CAMK2B	3	10.0%	Calcium/CaM-dependent protein kinase
O00743	PPP6C	3	8.8%	Catalytic subunit of protein phosphatase 6
Q92667	AKAP1	3	5.0%	Binds to regulatory subunits of protein kinase A
Cytoskeleton-related and centrosomal proteins				
Q15691	**EB1 (MAPRE1)**	**22**	**40.3%**	**EB1; associates with the plus end of microtubules and regulates microtubule cytoskeleton; binds STIM1**
B4DXP9	ACTR1A	11	21.3%	Involved in microtubule based vesicle motility; Associates with centrosome
F5H223	**DCTN2**	**9**	**28.0%**	**Component of dynactin complex; involved in anchoring microtubules to centrosomes**
P50991	DCTN1	9	9.8%	Required for movement of vesicles and organelles along microtubules
Q9UHD1	**CHORDC1**	**7**	**24.9%**	**Regulates centrosome duplication; involved in stress response**
Q14247	**CTTN**	**6**	**13.7%**	**Organizes actin cytoskeleton; regulates cell migration**
Q5VU61	TPM3	6	27.8%	Binds to and stabilizes actin filaments; involved in calcium-dependent muscle contraction
Q5SW79	*CEP170*	*5*	*4.6%*	*Involved in microtubule organization; CEP170B is a positive hit in RNAi screening*
Q15654	TRIP6	4	12.8%	Promotes actin cytoskeleton reorganization and cell invasiveness
Q8N8S7	ENAH	3	8.3%	Actin-associated proteins involved in cytoskeleton remodeling and cell polarity
Q9UJW0	DCTN4	3	6.1%	Component of the dynactin complex
Membrane protein transport and trafficking				
Q15437	**SEC23B**	**13**	**14.6%**	**Component of the COPII coat**
Q15436	**SEC23A**	**38**	**23.0%**	**Component of the COPII coat**
A6NG51	SPTAN1	7	4.4%	Contains 3 EF-hands involved in the calcium-dependent movement of the cytoskeleton
Q99653	CHP1	6	36.9%	*Calcineurin B homologous protein with 4 EF-hands; involved in* regulation of vesicular trafficking
F5H4L7	**VPS26A**	**5**	**19.0%**	**Component of the retromer complex; Regulates transcytosis of pIgR-pIgA**
Q8WUM4	**PDCD6IP**	**4**	**10.1%**	**Calcium-binding protein involved in regulation of apoptosis and proliferation; component of the endosomal sorting complex required for transport**
M0R061	*COPE*	*3*	*14.4%*	*Involved in biosynthetic protein transport; Positive hit from RNAi screening*
P40222	TXLNA	3	11.2%	Involved in intracellular vesicle traffic and calcium-dependent exocytosis in neuroendocrine cells
Q9P0L0	VAPA	3	11.2%	May play a role in vesicle trafficking
C9J8P9	**CLTA**	**3**	**10.7%**	**Intracellular protein transport**
C9JL73	ATP6V1B1	3	8.9%	Component of vacuolar ATPase
Q96QK1	VPS35	3	6.0%	Essential component of the retromer complex
F8VQP2	ATXN2	3	4.8%	Involved in EGFR trafficking
Q9Y678	*COPG*	*3*	*4.3%*	*Coatomer subunit gamma-1; Positive hit from RNAi screening*
Molecular chaperones				
P11021	**GRP78 or HSPA5**	**32**	**38.2%**	**Functions as a calcium-binding ER chaperone protein that could relocate from ER to cell surface upon stimulation with thapsigargin; Modulates ER stress and ER calcium leak;**
B4DYH1	HSPH1	9	12.7%	Molecular chaperones that mediate protein folding
P51572	BCAP31	5	16.7%	Multi-pass ER-resident; functions as a chaperone protein
Gene expression & translation regulation				
Q7Z417	NUFIP2	5	11.2%	Interacts with fragile X mental retardation (FMR)-interacting protein
Q7L576	CYFIP1	5	4.8%	Component of the CYFIP1-EIF4E-FMR1 complex which binds to the mRNA cap and mediates translational repression; part of the WAVE complex that regulates actin filament reorganization
E9PLT0	**CSDE1**	**4**	**8.8%**	**Involved in translationally coupled mRNA turnover**
Q7Z2W4	ZC3HAV1	3	5.1%	Recruits the cellular RNA degradation machineries to degrade the viral mRNAs

* Proteins identified under both store full and store depleted (1 μM TG+ 0 mM Ca medium) conditions were shown in bold. Candidates emerged from both the proteomic study and the RNAi screening (ref 11) were shown in italic.

siRNA screening for modulators of the NFAT pathway performed in Hela cells in ref 11.

Supplementary Table 2. Top candidates emerged from proteomic mapping of protein complexes surrounding STIM1 via *in situ* APEX2-catalyzed biotin labeling after store depletion*

UniProt ID	Gene Name	Spectral counts	Sequence coverage	Annotated/ reported functions & other remarks
ER or PM-resident proteins				
Q13586	***STIM1***	***159***	***46.6%***	***Activator of ORAI channels;*** ***Positive hit from RNAi screening#***
Q86TL2	***TMEM110 (STIMATE)***	***4***	***10.2%***	***Multi-pass membrane protein;*** ***Positive hit from RNAi screening***
Q15293	RCN1	4	7.9%	ER luminal calcium binding protein contains 6 EF-hands
Q96D31	*ORAI1*	*3*	*4.3%*	*Pore subunit of the CRAC channel; Positive hit from RNAi screening*
H7C4H2	**SRPRB**	**2**	**11.9%**	**Component of the signal recognition particle receptor**
F5H313	CACNA1D	2	5.4%	Alpha 1D subunit of L type voltage-dependent calcium channel $Ca_v1.3$; STIM1 inhibits its activity
Q9BSJ8	ESYT1	2	2.2%	Binds calcium via its C2 domains and translocates to sites of ER-PM contact in response to increased cytosolic calcium levels; Promotes the formation of ER-PM appositions
Posttranslational modifications (PTM) enzymes				
P55072	VCP	144	57.2%	Involved in ubiquitination and ER-association protein degradation
F5GZP3	***TRIM59***	***42***	***37.8%***	***Potential E3 ligase involved in ubiquitination;*** ***Positive hit from RNAi screening***
B4DV00	**PRMT5**	**19**	**17.4%**	**Arginine N-methyltransferase; PRMT depletion suppresses NFAT-dependent IL-2 production**
Q9HB71	CACYBP	13	25.9%	Involved in calcium dependent ubiquitination and proteosomal degradation of target proteins
O15269	**SPTLC1**	**2**	**2.3%**	**ER-resident; involved in serine palmitoylation**
Cytoskeleton-related processes				
Q15691	**MAPRE1 (EB1)**	**22**	**31.3%**	**Associates with the plus end of microtubules and regulates microtubule cytoskeleton; binds STIM1**
F5H223	**DCTN2**	**20**	**25.4%**	**Component of dynactin complex; involved in anchoring microtubules to centrosomes**
E7EVA0	*MAP4*	*17*	*4.0%*	*Interacts with SEPT2 and promotes microtubule assembly; Positive hit from RNAi screening*
Q14247	**CTTN**	**12**	**12.2%**	**Organizes actin cytoskeleton; regulates cell migration**
Q15019	*SEPT2*	*7*	*12.1%*	*Required for normal organization of the actin cytoskeleton; Septins identified as SOCE regulators in siRNA screening*
P46821	MAP1B	6	1.9%	Involved in maintaining microtubule stability
E9PPQ5	**CHORDC1**	**5**	**26.6%**	**Regulates centrosome duplication; involved in stress response**
E7EPK1	*SEP7*	*5*	*11.9%*	*Required for normal organization of the actin cytoskeleton; Septins identified as SOCE regulators in siRNA screening*
Q01518	CAP1	5	5.9%	Involved in actin cytoskeleton organization
K7EJ51	*SEPT9*	*2*	*11.2%*	*Required for normal organization of the actin cytoskeleton; Septins identified as SOCE regulators in siRNA screening*
D6RER5	*SEPT11*	*2*	*4.4%*	*Required for normal organization of the actin cytoskeleton; Septins identified as SOCE regulators in siRNA screening*
Membrane protein transport and trafficking				
Q00610	CLTC	39	10.0%	Assembly of coated pits
Q92734	TFG	34	33.0%	Involved in ER export and oncogenesis
F5H365	**SEC23A**	**29**	**21.9%**	**Component of the COPII coat**
Q15437	**SEC23B**	**10**	**9.8%**	**Component of the COPII coat**
B4DZT2	*STAM*	*8*	*6.1%*	*Component of the ESCRT complex; Positive hit from RNAi screening*
E9PLL0	MVB12A	5	24.8%	Component of the ESCRT-1 complex
Q8WUM4	**PDCD6IP**	**5**	**6.0%**	**Calcium-binding protein involved in regulation of apoptosis and proliferation; component of the endosomal sorting complex required for transport machinery**
O95721	SNAP29	4	14.0%	Involved in SNAP complex formation
O75436	**VPS26A**	**4**	**9.5%**	**Component of the retromer complex; Regulates transcytosis of pIgR-pIgA**
Q9UJZ1	STOML2	3	8.7%	Enriched in the immunological synapse in activated T cells; regulation of TCR signaling
C9J8P9	**CLTA**	**3**	**16.3%**	**Intracellular protein transport**
Q9UNF0	PACSIN2	3	4.5%	A lipid binding protein involved in the tabulation of membrane and vesicle-mediated protein transport
Q9H9H4	VPS37B	3	7.7%	Component of the ESCRT-1 complex; Regulator of vesicular trafficking process
P53618	*COPB1*	*3*	*2.5%*	*Involved in biosynthetic protein transport; Positive hit from RNAi screening*
Q9BXB4	OSBPL11	3	1.5%	Involved in lipid binding and transfer
Molecular chaperones and redox regulation				
P11021	**GRP78 or HSPA5**	**97**	**42.7%**	**Functions as a calcium-binding ER chaperone protein that could relocate from ER to cell surface upon stimulation with thapsigargin; Modulates ER stress and ER calcium leak;**
P14625	HSP90B1	3	2.7%	Functions as an ER chaperone protein; involved in ER-associated degradation (ERAD)
G3V448	TMX1	2	11.4%	Involved in redox regulation of ER
Gene expression & translational regulation				
Q12905	ILF2	6	12.1%	Regulate transcription of the IL-2 gene during T-cell activation
E9PLT0	**CSDE1**	**5**	**5.2%**	**Involved in translationally coupled mRNA turnover**
Others				
P49327	FASN	57	14.3%	Involved in synthesis of long-chain fatty acids
Q8NHR7	C15ORF43	3	14.5%	Function uncharacterized
Q9UPP5	KIAA1107	2	1.6%	Function uncharacterized

* Proteins identified under both store full and store depleted (1 μM TG+ 0 Ca medium) conditions were shown in bold. Candidates emerged from both the proteomic study and the RNAi screening (ref 11) were shown in italic.

siRNA screening for modulators of the NFAT pathway performed in Hela cells in ref 11.

Supplementary Table 3. DNASU clones (https://dnasu.org/DNASU/) used in the BiFc assay.

DNASU clone ID	Gene Symbol
HsCD00622598	*ORAI1*
HsCD00041259	*STIM1*
HsCD00510525	*TMEM110 (STIMATE)*
HsCD00042459	*PRMT5*
HsCD00080617	*CAMK2B*
HsCD00076084	*AKAP1*
HsCD00511701	*TRIM59*
HsCD00351705	*EB1 (MAPRE1)*
HsCD00041294	*DCTN4*
HsCD00622915	*SPTLC1*
HsCD00509136	*PPP6C*
HsCD00506889	*DCTN1*
HsCD00511194	*DCTN2*
HsCD00288073	*CHORDC1*
HsCD00513829	*CTTN*
HsCD00508876	*TPM3*
HsCD00508966	*CEP170*
HsCD00512262	*TRIP6*
HsCD00505652	*SEC23B*
HsCD00509322	*VPS26A*
HsCD00505816	*PDCD6IP*
HsCD00509109	*COPE*
HsCD00513383	*TXLNA*
HsCD00507814	*VAPA*
HsCD00507383	*CLTA*
HsCD00513049	*ATP6V1B1*
HsCD00505701	*VPS35*
HsCD00516363	*COPG*
HsCD00507928	*BCAP31*
HsCD00505788	*HSPH1*
HsCD00510884	*ACTR1A*
HsCD00296615	*ESYT1*
HsCD00513542	*VCP*
HsCD00041659	*STOML2*
HsCD00296111	*OSBPL11*
HsCD00509357	*SEPT2*
HsCD00509992	*RCN1*
HsCD00505971	*MAP4*
HsCD00511213	*TFG*
HsCD00511293	STAM

Supplementary Table 4. Sequences for siRNA oligos and list of primers used for qPCR.

siRNA oligonucleotides (oligos):

control siRNA oligo: 5'-UAAGGCUAUGAAGAGAUAC-3'

siSTIMATE #1: 5'-GACAAUUUCCUCAUGAGAA-3'

siSTIMATE #2: 5'-AGACGUCCGUGGAGGAUAU-3'

siSTIM1: 5'-GGUGGUGUCUAUCGUUAUU-3'

sgRNA designed to disrupt TMEM110 using CRISPR/Cas9

forward primer: 5'-CACCGGCATGCTGCTCATCTACGTG-3'

reverse primer: 5'-AAACCACGTAGATGAGCAGCATGCC-3'

The genomic region flanking the CRISPR/Cas9 target site for *TMEM110* was PCR amplified by using the following primers:

human TMEM110 forward: 5'-CCAGGGTGGTGTCTATCTCC-3';

human TMEM110 reverse: 5'-CCAGAACAGCCCCCTCTACC-3'.

qPCR primers used to exmaine TMEM110 distribution in human and mouse tissues:

target gene expression values were normalized to hGAPDH or mGAPDH.

hGAPDH forward primer: 5´-GTCTTCACTACCATGGAGAAGG-3'

hGAPDH reverse primer: 5´-TCATGGATGACCTTGGCCAG-3'

hTMEM110 forward primer: 5´- CGGCGAATATGGAGACCCTC-3'

hTMEM110 reverse primer: 5´-GGTTTTCAATGGGATTCAACAGG-3'

mGAPDH forward primer: 5´-AGGTCGGTGTGAACGGATTTG-3'

mGAPDH reverse primer: 5´-TGTAGACCATGTAGTTGAGGTCA-3'

mTMEM110 forward primer: 5'-GCGCTCATGCACAGTTTCG-3'

mTMEM110 reverse primer: 5'-ACAGTGAACAAGGGTCCTCTT-3'

Supplementary Video Legends

Supplementary Video 1 Side-by-side comparison of the time course of GFP-STIM1 puncta formation in normal HEK293 (WT, left) and STIMATE knockout HEK293 cells (STIMATE-KO, right) under TIRF microscope. The total fluorescence intensities of these two cells were comparable under epifluorescence microscope. Appended in the movie includes the time points after TG (1 μM)-induced store depletion.

Supplementary Video 2 Light-inducible accumulation of LiMETER at cortical ER in normal HEK293 (WT, left) and STIMATE knockout HEK293 cells (STIMATE-KO, right) under TIRFM**.** Appended in the movie includes the time points after light stimulation at 488 nm.